



An Investigation into the Free Vibration of Intact and Cracked FGM Plates

Mohamed B. Shehab · Moustafa S. Taima · Hussein Sayed · Tamer A. El-Sayed

Submitted: 3 April 2023 / in revised form: 5 August 2023 / Accepted: 15 August 2023
© The Author(s) 2023

Abstract In this study, the linear free vibration of intact and cracked functionally graded material plates is investigated numerically and experimentally. The experimental work is limited to the isotropic materials. The numerical work is based on finite element, where a code is developed to obtain the natural frequencies of intact plates based on the first-order shear deformation theory (FSDT) using MATLAB software. Also, a model of through-cracked FGM plate is developed using ANSYS Workbench with the help of APDL coding. The material properties of the plates under study are graded in one, two, and three directions. The novelty of this study emerges through its examination of the synergistic impacts resulting from variations in FGM material properties, crack length, crack orientation, and crack location. These effects are comprehensively discussed in the results section. The result of the present model shows that the use of three-directional FGM reduces the natural frequency compared with the other cases of two-directional and unidirectional FGM. Also, the

results show that the effect of FGM gradient on the frequency of intact and cracked plate is high when the gradient index $n < 3$. The present paper results are useful for the design of FGM plates especially when cracks exist.

Keywords FGM · Through cracks · Plates · ANSYS · Finite element · Free vibration · Experimental analysis · FSDT

Abbreviations

a	Plate length or dimension in the x -direction
b	Plate width or dimension in the y -direction
$[B]$	Strain-displacement matrix
$[B_b^e], [B_s^e]$	Strain-displacement matrix for bending and shear
c	Crack length
d	Vertical distance from the horizontal lower edge of the plate to the crack center
dA_e	Area of the element
D_{iso}	Flexural rigidity of the plate
$[D]$	Material constants matrix
$[D_b], [D_s]$	Material constants matrices for bending and shear
E	The modulus of elasticity at any point in the FGM plate
E_m, E_c	Modulus of elasticity of the metal and ceramic materials
h	Plate thickness
K^e	Element stiffness matrix
$[K]$	Global stiffness matrix
M^e	Element mass matrix
$[M]$	Global mass matrix
n	Material gradient index or volume fraction exponent

M. B. Shehab · M. S. Taima · H. Sayed · T. A. El-Sayed (✉)
Helwan University, Helmeiat-Elzaton, Cairo, Egypt
e-mail: Tamer.el-sayed@abdn.ac.uk

M. B. Shehab
e-mail: mohamed.bakry@m-eng.helwan.edu.eg

M. S. Taima
e-mail: moustafa.samir@m-eng.helwan.edu.eg

H. Sayed
e-mail: husseinsayed2008@m-eng.helwan.edu.eg

T. A. El-Sayed
University of Aberdeen, Aberdeen, UK

T. A. El-Sayed
University of Hertfordshire Hosted by GAF, New Admin
Capital, Cairo, Egypt

n_x, n_y, n_z	Material gradient index in x -direction, y -direction, and z -direction
$[N_i]$	Shape functions matrix
u, v, w	Displacement of a point in the plate along x -, y -, and z -directions
U^e	Strain energy stored in an element
V_c	Ceramic volume fraction
x, y, z	The coordinates of a point along the x -, y -, and z -directions in the plate
$\{\delta\}$	Nodal displacements vector
δ_c	Dimensionless crack position ratio
$\{\varepsilon\}$	Strain tensor
$\varepsilon_{xx}, \varepsilon_{yy}$	Normal strain components in x - and y -directions
ε_{xy}	In-plane shear strain component in $x - y$ plane
γ_{xz}, γ_{yz}	Out-of-plane shear strain component in $x - z$ and $y - z$ planes
θ_x, θ_y	Rotations about the x -axis and y -axis, respectively
κ	Shear correction factor
ν	The Poisson's ratio at any point in the FGM plate
ν_m, ν_c	Poisson's ratio of the metal and ceramic materials
ξ	Dimensionless crack length ratio
ρ	The density at any point in the FGM plate
ρ_m, ρ_c	Density of the metal and ceramic materials
$\{\sigma\}$	Stress tensor
σ_{xx}, σ_{yy}	Normal stress components in x - and y -directions
σ_{xy}	In-plane shear stress component in $x - y$ plane
τ_{xz}, τ_{yz}	Out-of-plane shear stress component in $x - z$ and $y - z$ planes
$\omega, \hat{\omega}$	Dimensional natural frequency of the plate H_z and $\frac{\text{rad}}{\text{sec}}$, respectively
$\Omega_{\text{iso}}, \Omega_{\text{FGM}}$	Dimensionless natural frequency of isotropic and FGM plates, respectively

Introduction

Plates are essential engineering components vastly used in several industrial applications such as shipbuilding, automotive and aerospace industries, and civil steel constructions. Due to the continuous advances in modern industries, the necessity to develop new materials, which are capable of functioning in harsh working conditions, is

increased. This led to designing new materials like functionally graded materials (FGMs) that can be tailored to obtain particular properties according to the required application [1]. FGM plates are made of two or more materials, usually metals and ceramics. The properties of these plates vary continuously along a specific plate dimension according to the volume fraction of the constituent materials.

The presence of cracks alters the response of plates to loads and shortens the expected service life of the used plates. Cracks may appear in plates during the manufacturing process or due to cyclic loading. Consequently, investigating the static and dynamic behavior of cracked plates becomes vital to ensure their effectiveness and reliability in different applications.

The static and dynamic analysis of intact (uncracked) plates was intensively investigated in many textbooks [2–5]. Mainly, the governing equations to obtain deflections and natural frequencies of plates are based on several theories with different assumptions. The most common plate theories are the classical plate theory (CPT) or Kirchhoff–Love plate theory and the Mindlin plate theory or the first-order shear deformation theory (FSDT). The CPT assumes that a plate section taken normal to the plate's middle surface remains plane and normal after the deformation neglecting the transverse shear deformation effect. Consequently, the CPT yields reasonable results for thin plates. On the other hand, the CPT is not valid for thick plates. The FSDT, which includes the transverse shear deformation effect, is used for moderately thick plates instead [6]. The assumption of the section perpendicular is relaxed in the FSDT theory. In the FSDT, the transverse shear stress distribution is constant, which contradicts the actual distribution. This issue is a result of assumed constant shear strains. However, shear correction factors are introduced into the shear stress resultants to correct the discrepancy. On the contrary, the higher-order shear deformation theory (HSDT) eliminates the necessity to use shear correction factors by introducing higher-order polynomial displacement functions [7–10]. The assumed functions cause the plate sections to be no longer straight after deformation. Higher-order deformation theories add a slight increase in accuracy at the cost of significantly increased complex equations and computational effort. That is why theories higher than the third-order shear deformation theory (TSDT) are less preferable unless the additional accuracy is required.

There is a large volume of publications that discuss the static and vibration analysis of cracked plates made of isotropic, orthotropic, and functionally graded material

(FGM). The most crack types that can be seen in these publications are part-through surface cracks, through cracks, all-over part-through cracks, side cracks, and internal cracks. Different approaches were attempted to perform the analysis either theoretically, experimentally, or both. The theoretical analysis can be done using analytical, variational iteration method [11] or numerical methods. The analytical solution for such problem is more involved and requires a lot of approximation to reach an analytical form [12–15]. Numerous publications studied static and vibration analysis of plates containing a part-through crack using an approximate analytical solution called the line spring model (LSM). The LSM was initially proposed by Rice and Levy [16], while studying a thin center-cracked isotropic rectangular plate under uniform tension and moment. The LSM treats the crack as a continuous line having compliance coefficients. Delale and Erdogan [17] modified the LSM obtaining the stress intensity factors (SIFs) of surface cracks in thick plates by including the transverse shear deformation. SIFs were obtained for plates subjected to different loading conditions. Mode I and III SIFs of a plate with an inclined surface crack under biaxial loading conditions were determined by Zhao-Jing and Shu-Ho [18]. Joseph and Erdogan [19] obtained SIFs for mode II and III of a cracked plate subjected to antisymmetric loading conditions. The LSM was utilized by several researchers to study the dynamic characteristics of part-through-cracked plates. In these publications, Berger's formulation and Galerkin's method were employed to transform the governing equation of the cracked plate to a nonlinear Duffing equation. The Duffing equation can be solved according to the multiple scale's approximate solution method. Israr, et al. [20] investigated a part-through center-cracked isotropic plate under tension and moment loads. The study illustrated the effect of both crack length and plate geometry on the natural frequency for three different boundary conditions. Following the same solution method, Ismail and Cartmell [21] and Bose and Mohanty [22] discussed a model of a variably oriented surface cracked thin plate. In the former research article, a plate under tension and moment loads is studied. In the latter research article, the effects of a combination of biaxial tension, bending, shear, and twisting stresses on a cracked plate with arbitrary orientation and position are investigated. Both articles illustrated the effect of crack orientation angle on the frequency. Thin orthotropic cracked plates were investigated by Joshi, et al. [23],

concluding that a crack located across the material fibres decreases the plate's natural frequency compared to a crack located along the fibres. Furthermore, the LSM can be utilized to analyze the dynamic characteristics of FGM plates, where the gradient of the material is along the thickness direction. An internally cracked rectangular thin FGM plate was studied by Joshi, et al. [24]. Gupta, et al. [25] replaced the internal crack with a partial-through crack. Their results show the effect of crack length, crack orientation, plate thickness, and gradient index on the fundamental frequency of the plate. The research on the same plate model was extended by Gupta, et al. [26] to include the effect of the thermal environment. In addition to the thermal environment, Soni, et al. [27] added fluid forces representing a fluid medium surrounding the plate model to study their effect on the dynamics of the FGM plate.

Several numerical methods were used for plate analysis in the published literature such as finite difference method [28–30], the Ritz method [31–35], the finite element method (FEM). The Ritz method was employed in several publications to study plates with side and internal cracks. Huang and Leissa [31] applied the Ritz method to study the free vibration of thin rectangular isotropic plates with side cracks of different locations, lengths, and orientations. Later, Huang, et al. [32, 33] modified their work to study thick side-cracked plates and internally cracked rectangular plates, respectively. The Ritz method was applied by Huang, et al. [34] and Uymaz, et al. [35] to investigate the effect of changing the volume fraction on natural frequencies and the mode shapes of FGM plates with property variation through plate thickness and in-plane directions, respectively.

It can be observed in the literature that the finite element method (FEM) is employed in many publications to analyze cracked structures. The ability of the FEM to model irregular geometries and the ease to apply boundary conditions gives FEM an advantage over other analytical methods. Several researchers applied FEM to study the dynamic response of plates with a center-through crack. Guan-Liang, et al. [36] constructed a finite element model of cracked plate using the integral of stress intensity factor. The natural frequencies of a simply supported and cantilever plate were obtained and compared to experimental ones for verification. Krawczuk and Gdansk [37, 38] obtained the flexibility matrix of a cracked plate finite element as a summation the flexibility matrix of uncracked

element to the flexibility matrix caused by the crack. The flexibility matrix is then used to get the stiffness matrix, thus obtaining the natural frequency of the plate. Side-cracked Mindlin plates were also studied by Azam, et al. [39] using FEM. They investigated the effect of crack length and orientation on the dynamic behavior of a square isotropic cracked plate for various boundary conditions.

Plates made of functionally graded material were the subject of various publications, and the majority of the analysis in these publications is done using FEM. Reddy [40] presented Navier's solutions and a finite element model to study the static and dynamic behavior of FGM plates. Talha and Singh [41] developed higher-order shear deformation theory with a special modification in the transverse displacement to study the static and the dynamic response of FGM plates. Minh, et al. [42, 43] employed Shi's high-order shear deformation theory [44], the phase field theory, and FEM to study the free vibration of a cracked FGM with variable thickness. Also, Minh and Duc [43] considered temperature-dependent material properties through the thickness direction in their study.

A major problem that faced the traditional FEM when modeling crack growth problems is the necessity to repeat the meshing process to adapt to the change in the dimensions of the discontinuity. The extended finite element technique (X-FEM) [45] was proposed by Belytschko and Black [46] to overcome the drawbacks of the traditional FEM. The authors studied the elastic fracture propagation relying on the partition of the unity property noted by Melenk and Babuška [47]. In X-FEM, the geometry is discretized using the conventional FEM; then enrichment functions of nodal elements containing the crack are added. Moës, et al. [48] enhanced the work of Belytschko and Black [46] by introducing the Heaviside function to model the crack away from the crack tip. A number of researchers employed the X-FEM in their work concerning vibrational studies. Bachene, et al. [49, 50] applied X-FEM to study the vibration of Mindlin isotropic plates with side- and center-through cracks. The authors computed the non-dimensional fundamental frequency for different crack length values at different boundary conditions. Natarajan, et al. [51] studied FGM plates with properties vary in the thickness direction by a simple power law. The authors investigated the effect of the gradient index, crack location, crack length, crack orientation, and the thickness on the natural frequency of the FGM plate using 4-noded element with 20 degrees of freedom.

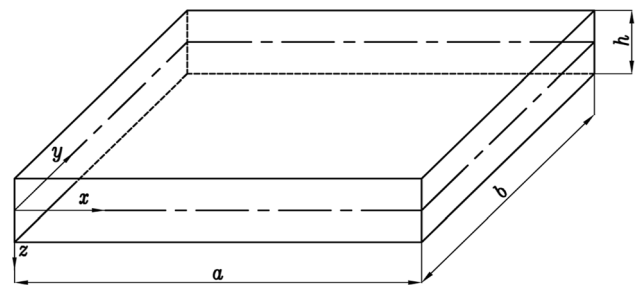


Fig. 1 The geometry and dimensions of an intact plate

Modeling a problem using the finite element method can also be done using commercial finite element software packages such as ANSYS, ABAQUS. The results from these simulation programs proved to be consistent with the analytical, numerical, and experimental results seen in the literature. Hosseini-Hashemi, et al. [52] used both the analytical method of LSM and ABAQUS software to study the free vibration of all over part-through isotropic plates. The authors investigated the effect of crack depth, crack location, and plate dimensions on the natural frequency. Nkounhawa, et al. [53] performed a modal analysis of a thin isotropic rectangular plate using both the method of separating the variables and ANSYS software. Pingulkar and Suresha [54] used ANSYS software to obtain the natural frequencies and the mode shapes of glass and carbon fiber-reinforced polymer composites. The authors discussed the effect of changing the matrix material, the stacking sequence, and the volume fraction on the natural frequency of the plate. Al-Shammari [55] investigated the effect of the crack length and orientation on the natural frequency of a cracked sandwich plate. The sandwich plate is made from stainless steel with Teflon core. He obtained the results numerically using ANSYS and then validated them experimentally. Modal analysis of a square intact FGM plate was performed by Tabatabaei and Fattahi [56] using ABAQUS coupled with FORTRAN code. The analysis is done for different values of material gradient indices where the material properties vary along the thickness of the plate according to the simple power law.

More recently, the rapid advancements in neural network and machine learning have opened up new possibilities for solving partial differential equations. Guo, et al. [57] solved the fourth-order biharmonic equation of Kirchhoff plates using the deep collocation method (DCM). Plates of various shapes subjected to different boundary conditions and loads were included in their study. In the study by [58], the authors studied the bending,

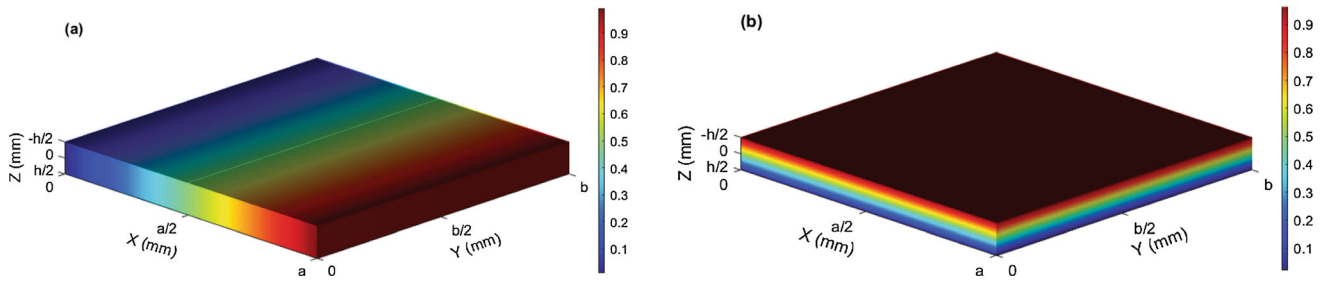


Fig. 2 A representation of a FGM square plate with a unidirectional variation of the volume fraction (V_c). The gradient index is taken to be 1.0 in each case. Figure (a) shows the variation through the x -direction, while figure (b) shows the variation through the z -direction.

The blue and red colors represent the metal and the ceramic-rich portion of the plate, respectively (Color figure online)

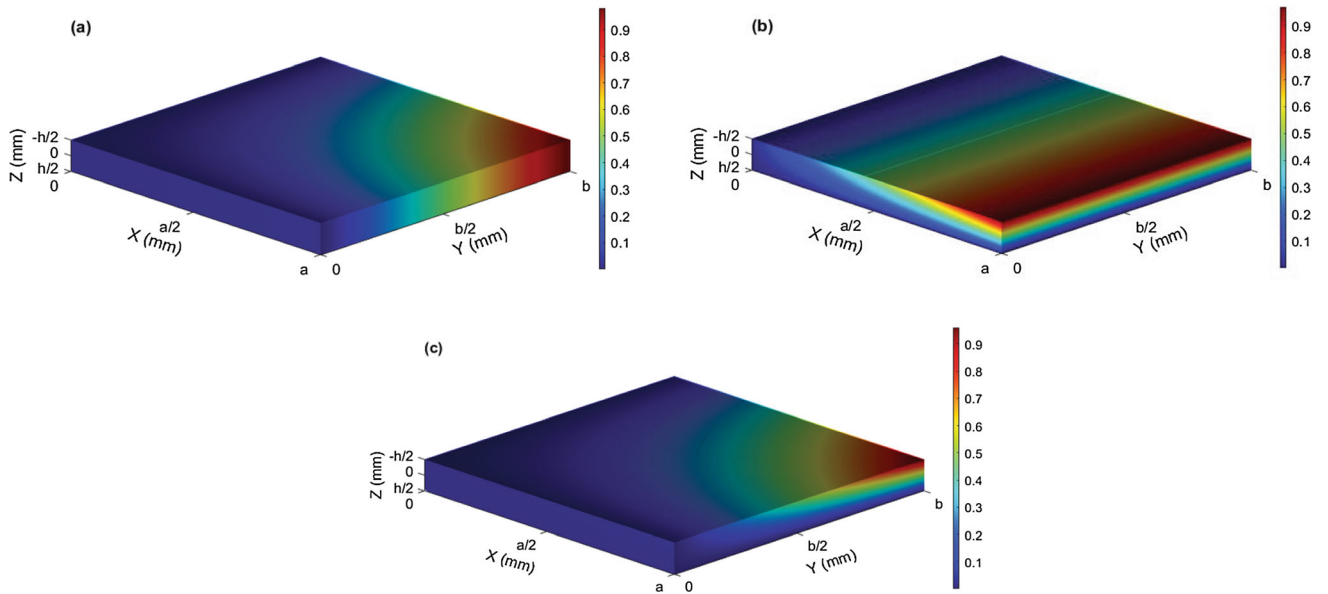


Fig. 3 A representation of a FGM square plate with a multidirectional variation of the volume fraction (V_c). The gradient index is taken to be 1.0 in each case. Figure (a, b) shows a two-directional variation across the $x - y$ plane and the $x - z$ plane, while the variation in figure (c) is a three-directional variation through the

x, y, z -directions simultaneously. The blue and red colors represent the metal and the ceramic-rich portion of the plate, respectively (Color figure online)

vibration, and buckling of Kirchhoff plates using deep autoencoder-based energy method (DAEM). Lastly, physics-informed neural network (PINN) algorithm was

proposed by Goswami, et al. [59] to solve several brittle fracture problems which included cracked plates.

From the previous literature, it can be realized the importance of investigation of cracked plates and the

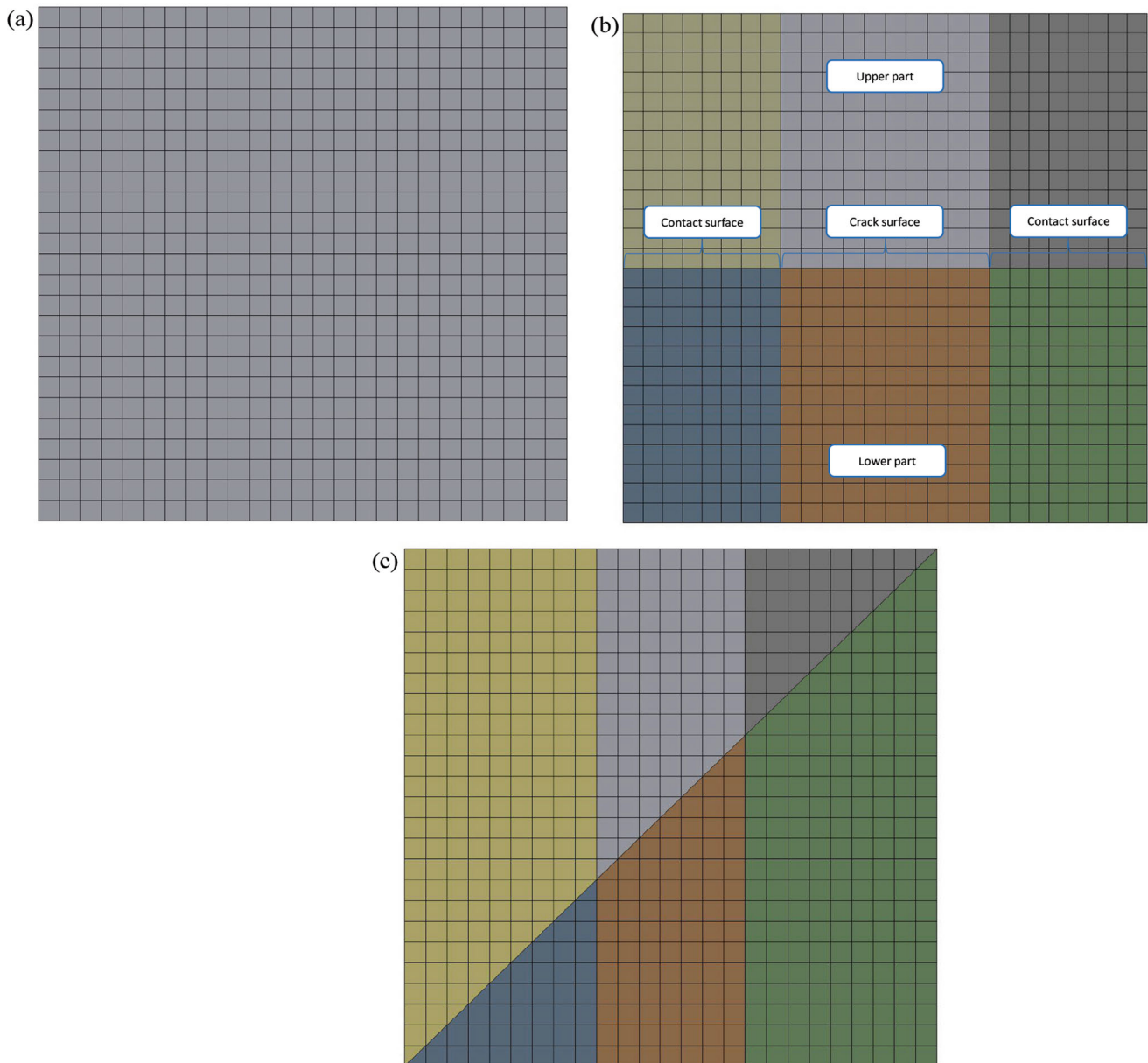


Fig. 4 Finite element discretization of intact and cracked plates using ANSYS mechanical. SOLID185 hexahedral elements are used for intact plates in figure (a), while a combination of hexahedral and wedge elements is used for cracked plates in figures (b, c)

investigation of new materials using function-graded materials and this is the main topic of the present paper. After this introduction, Section “[Theoretical Model and Experimental Analysis](#)” presents the theoretical formula-

tion based on FSDT, finite element model using ANSYS WORKBENCH, and experimental verification analysis. Then, Section “[Results](#)” presents the model verification results and the present new results. The effect of FGM

parameters and crack parameters on the dynamics of plate is investigated. Section “Results” includes also the discussion of these results. Finally, the remarkable results are presented in the conclusion section.

Theoretical Model and Experimental Analysis

Consider a functionally graded material plate made from a metal–ceramic mixture in the Cartesian coordinate system, as shown in Fig. 1. x , y , and z are the coordinates of a point along the x , y , and z direction in the plate. The plate dimensions in the x , y , and z directions are length (a), width (b), and thickness (h), respectively. In this study, the effect of changing the material properties gradient’s direction on the plate’s dynamic behavior is discussed. Different cases of the unidirectional and multi-directional variation of the ceramic volume fraction V_c , thus the material properties, can be displayed in Figs. 2 and 3. Power law distribution is used to describe the variation of material properties in these cases. In Fig. 2(a), the material properties are graded along the x -direction. The left surface ($x = 0$) is the metal-rich surface of the plate, while the ceramic-rich surface is at the right surface ($x = a$). Similarly, the material properties are graded along the z -direction in Fig. 2(b). The bottom surface ($z = \frac{h}{2}$) is the metal-rich surface of the plate, while the ceramic-rich surface is at the top surface ($z = \frac{h}{2}$). Two-directional variation of V_c through the $x - y$ and $x - z$ planes is illustrated in Fig. 3a and b. In the former figure, the properties are graded from the plate’s ceramic-rich portion at ($x = 0, y = 0$) to the metal-rich portion at ($x = a, y = b$). On the contrary, the variation is from the ceramic-rich portion of the plate at ($x = 0, z = \frac{h}{2}$) to the metal-rich portion at ($x = a, z = \frac{h}{2}$) in the latter figure. The ceramic volume fraction at a point in the plate can be expressed as:

$$V_c(x, y, z) = \frac{x^{n_x} y^{n_y} 2z + h^{n_z}}{a b 2h}, (n_x, n_y, n_z \geq 0), \tag{Eq 1}$$

where n_x, n_y , and n_z are the material gradient indices (or the volume fraction exponents) in the x, y, z -directions, respectively. The summation of the volume fractions of the metal and ceramic material must equal unity. According to the rule of mixtures, the modulus of elasticity E , the density ρ , and the Poisson’s ratio ν can be expressed as:

$$\begin{aligned} E(x, y, z) &= E_m + V_c(E_m - E_c), \\ \rho(x, y, z) &= \rho_m + V_c(\rho_m - \rho_c), \\ \nu(x, y, z) &= \nu_m + V_c(\nu_m - \nu_c), \end{aligned} \tag{Eq 2}$$

where the subscripts m and c indicate the metal and ceramic materials.

The displacement of a point in the plate along x, y, z -directions are u, v , and w , respectively. According to the FSDT, the displacement field can be expressed as:

$$\begin{aligned} u(x, y, z, t) &= -z\theta_y(x, y, t), \\ v(x, y, z, t) &= -z\theta_x(x, y, t), \\ w(x, y, z, t) &= w_0(x, y, t), \end{aligned} \tag{Eq 3}$$

where θ_x and θ_y denote rotations about the x -axis and y -axis, respectively. The linear strains corresponding to the displacement field can be written in a matrix form as:

$$\{\varepsilon\} = \begin{Bmatrix} \varepsilon_{xx} \\ \varepsilon_{yy} \\ \varepsilon_{xy} \\ \gamma_{xz} \\ \gamma_{yz} \end{Bmatrix} = \begin{Bmatrix} u_{,x} \\ v_{,y} \\ u_{,y} + v_{,x} \\ w_{,x} + u_{,z} \\ w_{,y} + v_{,z} \end{Bmatrix} = \begin{Bmatrix} -z\theta_{y,x} \\ -z\theta_{x,y} \\ -z(\theta_{y,y} + \theta_{x,x}) \\ w_{,x} - \theta_y \\ w_{,y} - \theta_x \end{Bmatrix}, \tag{Eq 4}$$

where the comma in the subscript denotes the partial derivative of the variable with respect to the following coordinate x, y , or z . The linear constitutive relation can be evaluated as the following:

$$\begin{Bmatrix} \sigma_{xx} \\ \sigma_{yy} \\ \sigma_{xy} \\ \tau_{xz} \\ \tau_{yz} \end{Bmatrix} = \begin{bmatrix} D_{b11} & D_{b12} & D_{b13} & 0 & 0 \\ D_{b21} & D_{b22} & D_{b23} & 0 & 0 \\ D_{b31} & D_{b32} & D_{b33} & 0 & 0 \\ 0 & 0 & 0 & D_{s11} & D_{s12} \\ 0 & 0 & 0 & D_{s21} & D_{s22} \end{bmatrix} \begin{Bmatrix} \varepsilon_x \\ \varepsilon_y \\ \varepsilon_{xy} \\ \gamma_{xz} \\ \gamma_{yz} \end{Bmatrix}, \tag{Eq 5}$$

or in a compact form as the following:

$$\{\sigma\} = [D]\{\varepsilon\},$$

where σ_{xx}, σ_{yy} , and σ_{xy} are the in-plane stresses, while τ_{xz} and τ_{yz} are the out-of-plane stresses. $D_{bij}(i, j = 1, 2, 3)$ and $D_{sij}(i, j = 1, 2)$ are the elements of the material constants matrices for bending and shear, respectively. $[D_b]$ and $[D_s]$ can be expressed as:

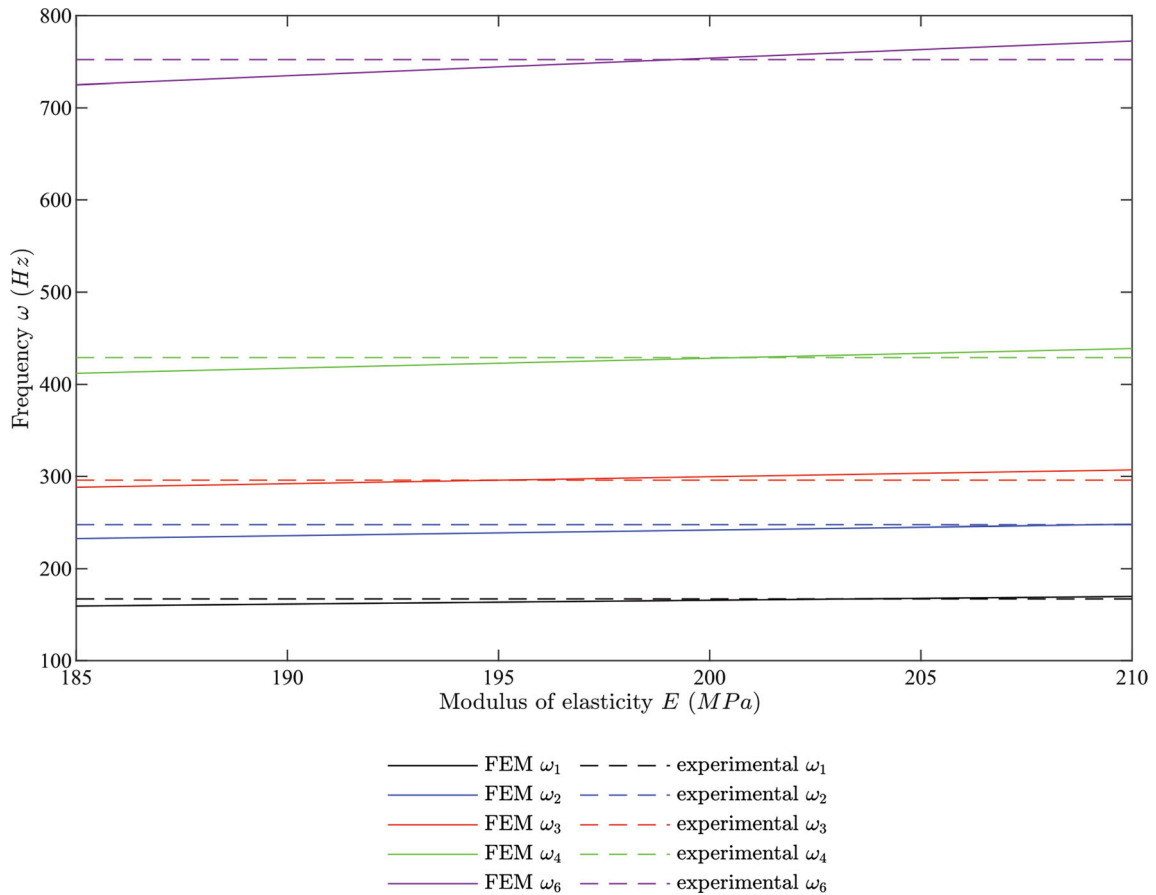


Fig. 5 The first six natural frequencies are obtained experimentally and by using the modal analysis in ANSYS software. The frequencies evaluated by the modal analysis, represented by solid lines, are evaluated for a range of elastic moduli (E). The experimentally

measured frequencies of the plate sample, whose the elastic modulus to be determined, are represented by dashed lines

$$D_b = \frac{E(x, y, z)}{1 - \nu^2(x, y, z)} \begin{bmatrix} 1 & \nu(x, y, z) & 0 \\ \nu(x, y, z) & 1 & 0 \\ 0 & 0 & \frac{1-\nu(x,y,z)}{2} \end{bmatrix} \text{ and}$$

$$D_s = \frac{E(x, y, z)}{2(1 + \nu(x, y, z))} \begin{bmatrix} 1 & 0 \\ 0 & 1 \end{bmatrix}. \tag{Eq 6}$$

The assumptions of the Mindlin plate theory reduce the three-dimensional plate problem into a two-dimensional one. The finite element discretization of the 2D plate's midplane forms quadrilateral elements. In this study, linear quadrilateral elements with three degrees of freedom (w, θ_y, θ_x) at each node are used. The displacement vector $\{\delta\}$ containing the degrees of freedom is given by:

$$\{\delta\} = \sum_{i=1}^k [N_i] \{\delta_i\}, \tag{Eq 7}$$

where $\{\delta_i\} = \begin{Bmatrix} w_i \\ \theta_{yi} \\ \theta_{xi} \end{Bmatrix}$.

N_i and δ_i are the shape functions and the nodal displacement for each node i . k is the total number of nodes in one element. Like Eq. 7, the stress and the strain fields in Eqs. 4 and 5 become:

$$\{e\} = [B_i^e] \{\delta_i\}, \{\sigma\} = [D][B_i^e] \{\delta_i\}, \tag{Eq 8}$$

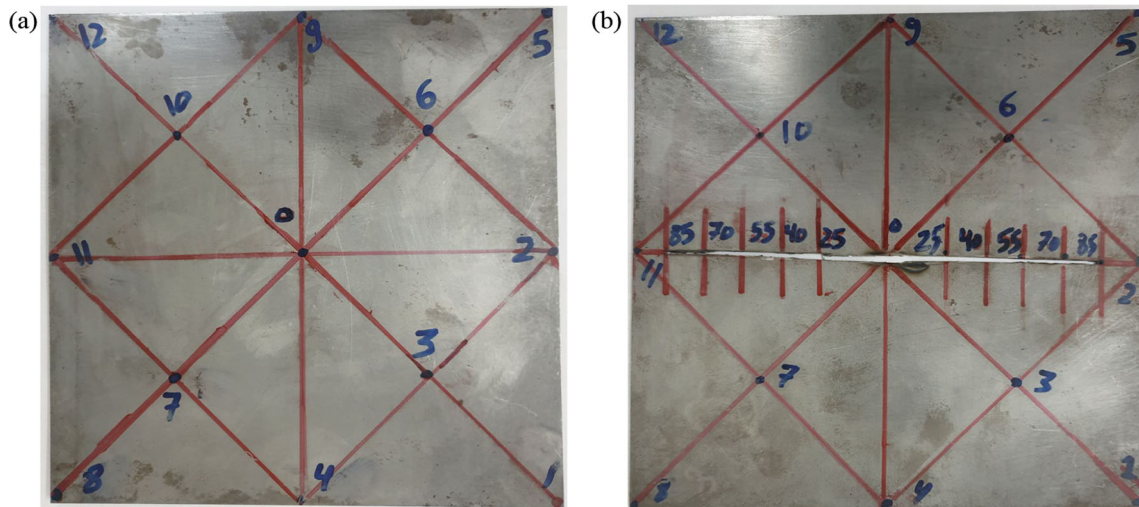


Fig. 6 Intact and cracked plate samples prepared for the experimental measurement of the natural frequency. Each sample is marked with thirteen points at equal distances. These points label the locations of impacting the plate with the hammer and mounting of the accelerometer

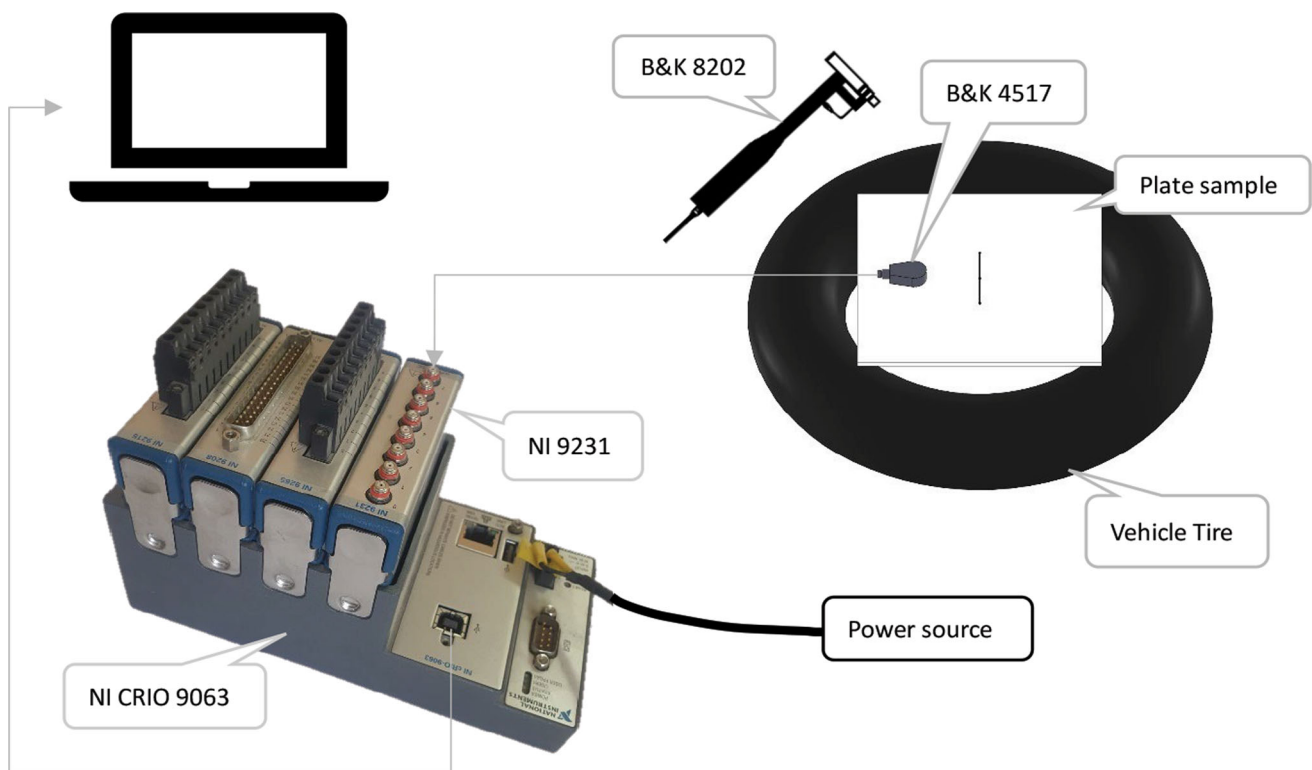


Fig. 7 Schematic diagram of the experimental setup used to measure the frequency of intact and cracked plate samples

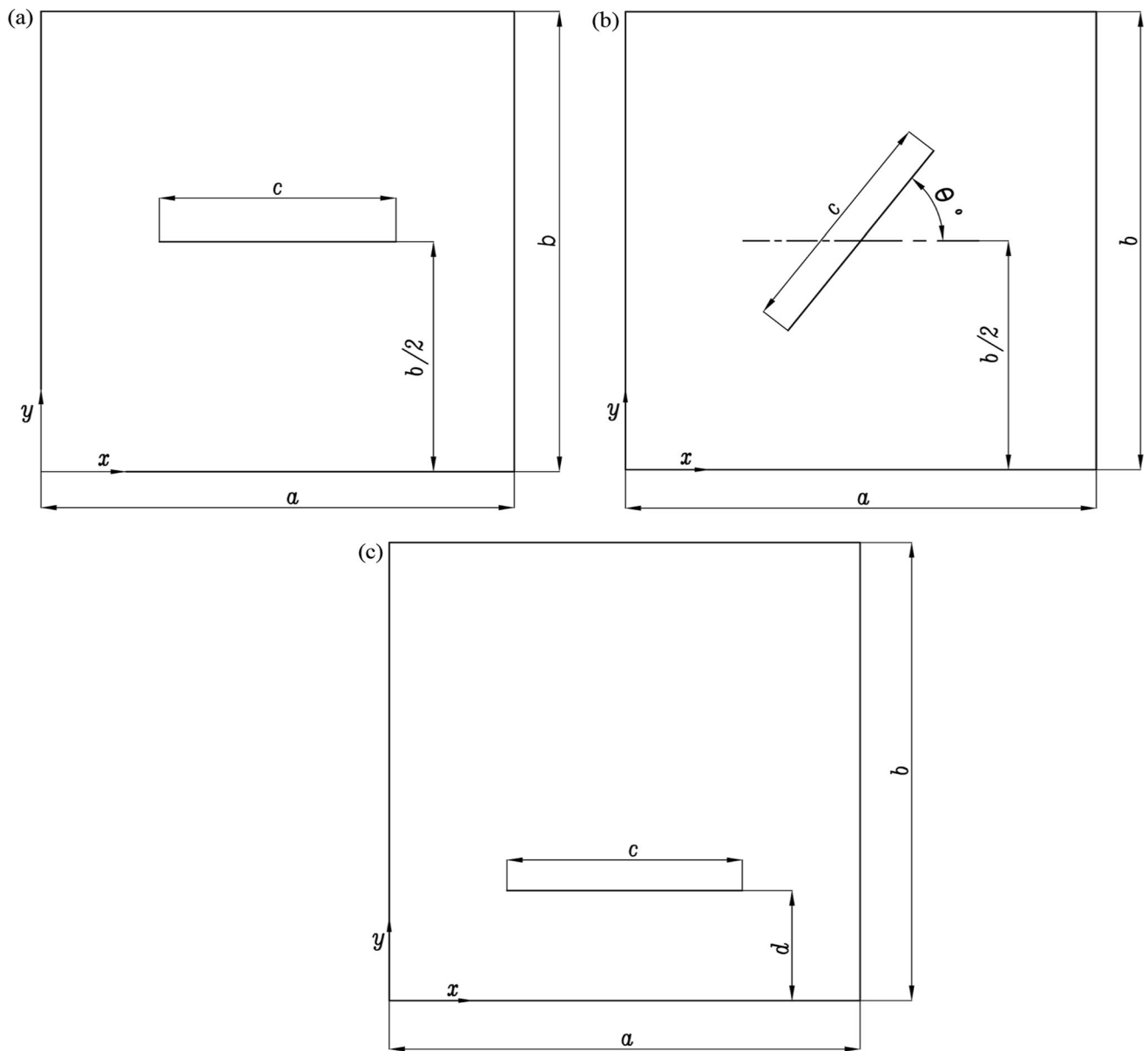


Fig. 8 The main dimensions of the FGM plates under study in the results section. The plates have different configurations of through cracks shown in figures (a–c) as the following (a) horizontally centre-cracked plate. The crack is parallel to the x -direction and has a length equal to c . (b) Slanted through crack at the center. The crack is at

angle (θ) with the x -axis direction and has a length equal to c . (c) Off-center-through crack. The crack has a length equal to c and at a distance d from the plate edge a

Table 1 A comparison between the dimensionless natural frequencies of a steel plate obtained from the FEM and the experimental setup for different dimensionless crack ratio (ξ)

ξ	Ω_i	Experimental	FEM (ANSYS)		ξ	Ω_i	Experimental	FEM (ANSYS)	
			SOLID185	SHELL181				SOLID185	SHELL181
0	Ω_1	13.6333	13.5689	13.5876	0.55	Ω_1	12.9503	13.5311	13.5613
	Ω_2	20.1912	19.8151	19.8192		Ω_2	16.5500	17.0714	17.1689
	Ω_3	24.1370	24.5381	24.5463		Ω_3	21.9920	22.1454	22.1740
	Ω_4	34.9833	35.0576	35.1084		Ω_4	31.8917	33.2631	33.3578
0.25	Ω_1	13.0526	13.5528	13.5769	0.7	Ω_1	13.0104	13.5131	13.5462
	Ω_2	18.7040	19.4278	19.4574		Ω_2	14.7466	15.0248	15.1461
	Ω_3	23.3236	23.6180	23.6703		Ω_3	21.5746	21.8816	21.8978
	Ω_4	33.6559	34.9817	35.0367		Ω_4	29.0195	29.8970	30.0446
0.4	Ω_1	12.9530	13.5429	13.5702	0.85	Ω_1	12.1281	12.5066	12.6605
	Ω_2	17.8559	18.5909	18.6535		Ω_2	13.3501	13.4818	13.5178
	Ω_3	22.5280	22.7278	22.7755		Ω_3	21.3802	21.7748	21.7855
	Ω_4	33.2024	34.5767	34.6431		Ω_4	24.0761	24.4705	24.6453

Table 2 The first four dimensionless natural frequencies of a simply supported (SUS304/Si3N4) FGM thick ($\frac{c}{h} = 10$) plate for different values of the gradient index across the thickness

		Gradient index						Mode
		Ceramic	0.5	1.0	5.0	10	Metal	
Current study	Talha and Singh [41]	5.7523	3.9701	3.4845	2.8351	2.6973	2.5154	1
	SOLID185	5.4433	3.7954	3.3295	2.7167	2.5891	2.4174	
	SHELL181	5.6807	4.1265	3.4884	2.5572	2.5106	2.5091	
	FDST	5.6846	4.1465	3.4908	2.5321	2.4841	2.5107	
Current study	Talha and Singh [41]	14.0336	9.6890	8.4903	6.8941	6.5669	6.1361	2
	SOLID185	13.2707	9.2401	8.0992	6.5891	6.2780	5.8661	
	SHELL181	13.5868	9.8605	8.3300	6.0963	5.9845	5.9809	
	FDST	13.6176	9.9169	8.3487	6.0558	5.9410	5.9941	
Current study	Talha and Singh [41]	14.0354	9.6906	8.4918	6.8952	6.5680	6.1370	3
	SOLID 185	13.2707	9.2401	8.0992	6.5891	6.2780	5.8661	
	SHELL 181	13.5868	9.8605	8.3300	6.0963	5.9845	5.9809	
	FDST	13.6176	9.9169	8.3487	6.0558	5.9410	5.9941	
Current study	Talha and Singh [41]	21.6188	14.9404	13.0959	10.6102	10.1053	9.4515	4
	SOLID185	20.1753	14.0529	12.3139	9.9922	9.5224	8.9142	
	SHELL181	20.8931	15.1514	12.7926	9.3494	9.1771	9.1718	
	FDST	20.9409	15.2297	12.8212	9.3000	9.1238	9.1917	

Table 3 The first four dimensionless natural frequencies of a clamped (SUS304/Si3N4) FGM thick ($\frac{d}{h} = 10$) plate for different values of the gradient index across the thickness

		Gradient index						
		Ceramic	0.5	1.0	5.0	10	Metal	Mode
Current study	Talha and Singh [41]	10.1599	7.0202	6.1489	4.9816	4.7457	4.4410	1
	SOLID185	9.7808	6.8068	5.9615	4.8367	4.6074	4.3079	
	SHELL181	9.7348	7.0599	5.9610	4.3570	4.2768	4.2742	
	FDST	9.7210	7.0699	5.9519	4.3172	4.2354	4.2671	
Current study	Talha and Singh [41]	19.9367	13.7978	12.0812	9.7440	9.2841	8.7107	2
	SOLID185	18.7497	13.0398	11.4074	9.2109	8.7742	8.2224	
	SHELL181	18.6331	13.4962	11.3849	8.3029	8.1487	8.1437	
	FDST	18.6335	13.5221	11.3837	8.2573	8.1008	8.1418	
Current study	Talha and Singh [41]	19.9367	13.7978	12.0812	9.7440	9.2841	8.7107	3
	SOLID185	18.7497	13.0398	11.4074	9.2109	8.7742	8.2224	
	SHELL181	18.6331	13.4962	11.3849	8.3029	8.1487	8.1437	
	FDST	18.6335	13.5221	11.3837	8.2573	8.1008	8.1418	
Current study	Talha and Singh [41]	28.1367	19.4845	17.0625	13.7350	13.0873	12.2919	4
	SOLID185	26.3634	18.3247	16.0204	12.8993	12.2873	11.5297	
	SHELL181	26.1717	18.9414	15.9689	11.6299	11.4128	11.4058	
	FDST	26.0777	18.8973	15.9089	8.2573	11.3210	11.3609	

Table 4 Properties of the constituents of the functionally graded material [51]

Material	Properties		
	E (GPa)	ρ (Kg/m ³)	ν
Stainless steel (SUS304)	201.04	8166	0.28
Silicon nitride (Si ₃ N ₄)	348.43	2370	0.28

where $[B_i] = \begin{bmatrix} 0 & -N_{i,x} & 0 \\ 0 & 0 & -N_{i,y} \\ 0 & -N_{i,y} & -N_{i,x} \\ N_{i,x} & -N_i & 0 \\ N_{i,x} & 0 & -N_i \end{bmatrix}$.

$[B_i^e]$ is the strain-displacement matrix. The first three rows form the bending strain-displacement matrix $[B_{bi}^e]$, while the last two rows are associated with shear forming $[B_{si}^e]$. The potential energy U^e of an element can be obtained as:

$$U^e = \frac{1}{2} \int_{-h/2}^{h/2} \int_{A_e} z^2 \delta_i^T [B_b^e]^T [D_b^e] [B_b^e] \delta_i^T dA_e dz + \frac{\kappa}{2} \int_{-h/2}^{h/2} \int_{A_e} \delta_i^T [B_s^e]^T [D_s^e] [B_s^e] \delta_i^T dA_e dz, \tag{Eq 9}$$

where A_e, κ is the area of the element and shear correction factor, respectively. The element stiffness matrix K^e and mass matrix M^e can be calculated from:

$$K^e = \frac{h^3}{12} \int_{A_e} [B_b^e]^T [D_b^e] [B_b^e] dA_e + \kappa h \int_{A_e} [B_s^e]^T [D_s^e] [B_s^e] dA_e, \tag{Eq 10}$$

$$M^e = \int_{A_e} \rho [N_i]^T [I] [N_i] dA_e, \tag{Eq 11}$$

where $[I] = \begin{bmatrix} h & 0 & 0 \\ 0 & \frac{h^3}{12} & 0 \\ 0 & 0 & \frac{h^3}{12} \end{bmatrix}$.

Numerical integration is used to solve Eqs. 10 and 11 to obtain the stiffness and mass matrix for each element. After that, the global stiffness matrix $[K]$ and mass matrix $[M]$ are then assembled by traditional technique. Finally, after applying boundary conditions, the natural frequencies of an intact plate in a free vibration mode can be obtained as the following:

$$([K] - \hat{\omega}^2 [M]) \{\delta\} = 0, \tag{Eq 12}$$

where $\hat{\omega}$ is the natural frequency of the plate.

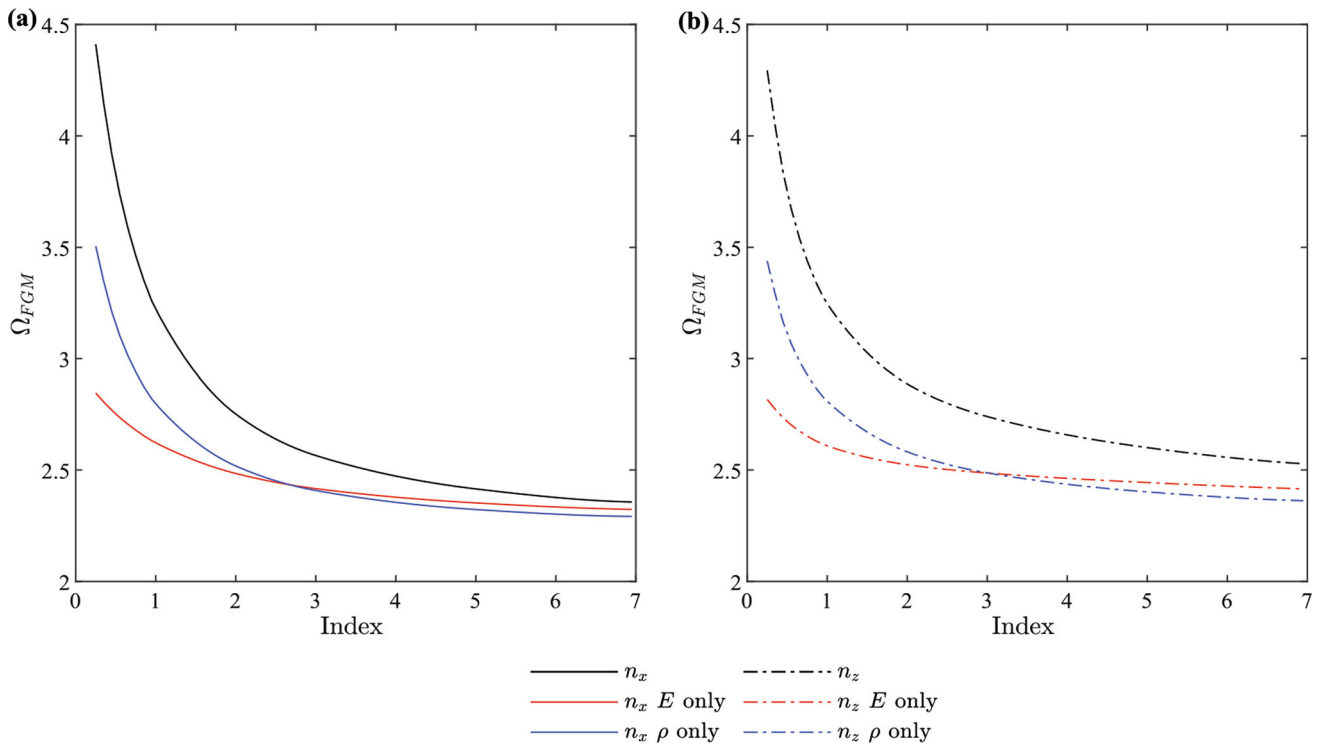


Fig. 9 The effect of varying the material properties (elastic modulus (E) and the density (ρ)) based on the variation of the gradient index in the x -direction (n_x) and the z -direction (n_z) on the dimensionless frequency (Ω_{FGM}) is represented by black lines in figures (a) and (b), respectively. Also, the effect of changing each of the elastic modulus

(E) and the density (ρ) properties separately on the frequency is presented in different colors in each figure. The plate under study is an intact, simply supported plate

Finite Element Model Using ANSYS

The dynamic analysis of intact and cracked FGM plates was performed using ANSYS software. The plate's geometry was created using the Design Modeler module provided in the ANSYS Workbench. Parameters under study, such as plate dimensions, crack length, crack location, and crack orientation, were implemented into the geometry as variables to control them through the Workbench's parametric table. Here, the regular shape of the intact plate efficiently permits filling the shape with eight-noded hexahedra regular solid elements (Solid 185); see Fig. 4a.

The functionally graded material properties were implemented in the model by inserting APDL commands that control the individual element material properties into Workbench's modal module. It is worth emphasizing that FGM properties are a function of the volume fraction V_c , which is a function of the coordinates x, y , and z ; see Eq. 1. The APDL code evaluates V_c at the coordinates of the centroid of each element. As a result, regular-shaped prism and hexahedral elements are used, which ensure uniform distribution of FGM properties. The FGM distribution in each direction could be manipulated by controlling the elements' size in x, y, z -directions. The APDL coding steps of the finite elements' selection and assignment of the

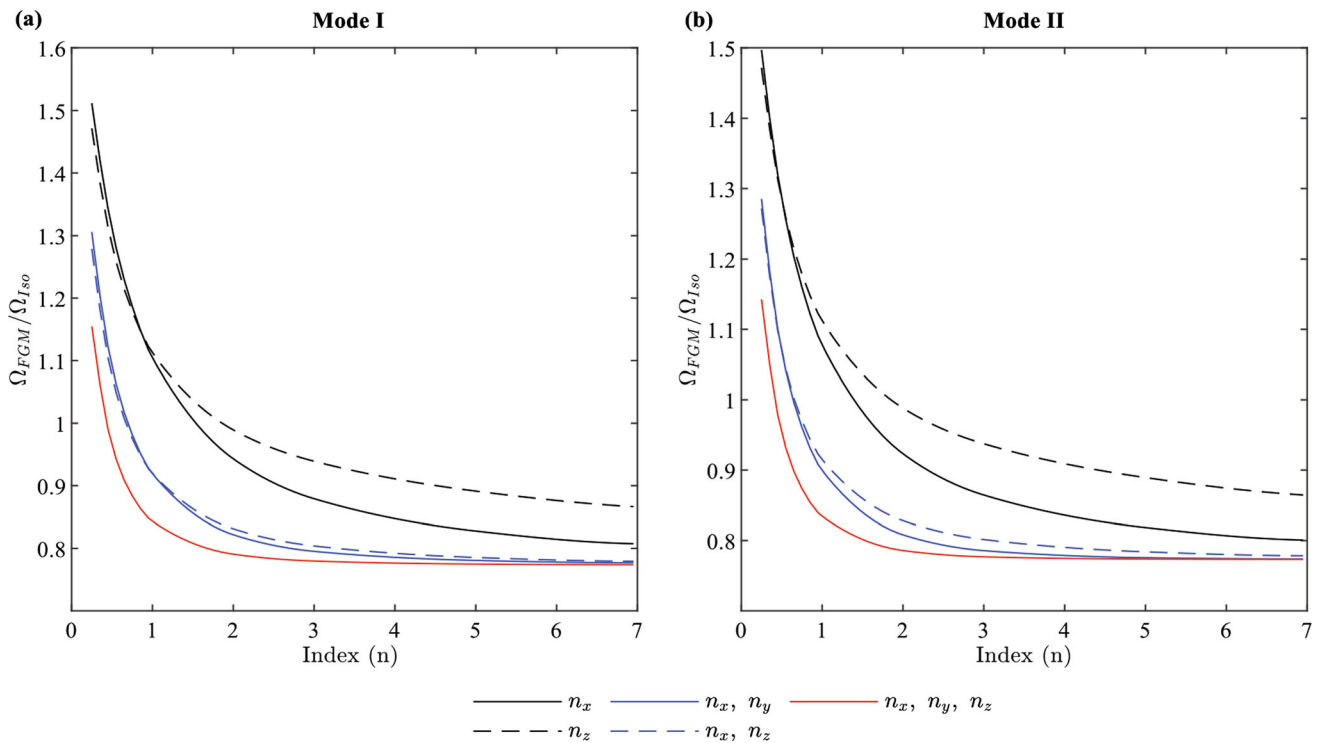


Fig. 10 The effect of changing the gradient index (n) on the dimensionless frequency ratio ($\frac{\Omega_{FGM}}{\Omega_{Iso}}$) of an intact plate. The figures (a, b) represent the first and second plate natural frequency, respectively. In each figure, the frequency ratio is plotted in three

different colors representing unidirectional, two-directional, and three-directional variation of the material properties (Color figure online)

corresponding material properties based on each element’s coordinates are illustrated in Fig.-17 in Appendix 1.

As for the case of the cracked plate, a plate geometry consisting of two parts, upper and lower, with a separating surface in between was created. Each part is divided into three zones. Then, the crack is defined by applying a “bonded contact” between the bodies of the outer zones leaving the middle contact surface free, see Fig. 4b and c. The crack length c is controlled by changing the bonded surfaces’ size. However, changing the crack geometry or orientation can cause disorder to the elements in the cracked plate model resulting in tetrahedron and irregular hexahedra elements. This disorder leads to nonuniform distribution of functionally graded material properties, which is undesirable.

Ensuring a uniform distribution of properties of the cracked plate is more challenging than the intact case. This

requires splitting bodies into smaller volumes that can be meshed into regular-shaped elements. Then applying mesh sizing controls to body edges to force generating hex and wedge elements. Clearly, accomplishing this task manually for different cases of crack length and orientation is a tedious process. Therefore, the process is coded using Workbench’s scripting to automatically create the required “named selections” required to group the edges to be meshed and to group the surfaces to apply contact.

Experimental Work

The aim of the experimental work is to validate the finite element model of cracked plate. However, the experimental work was limited to isotropic materials only.

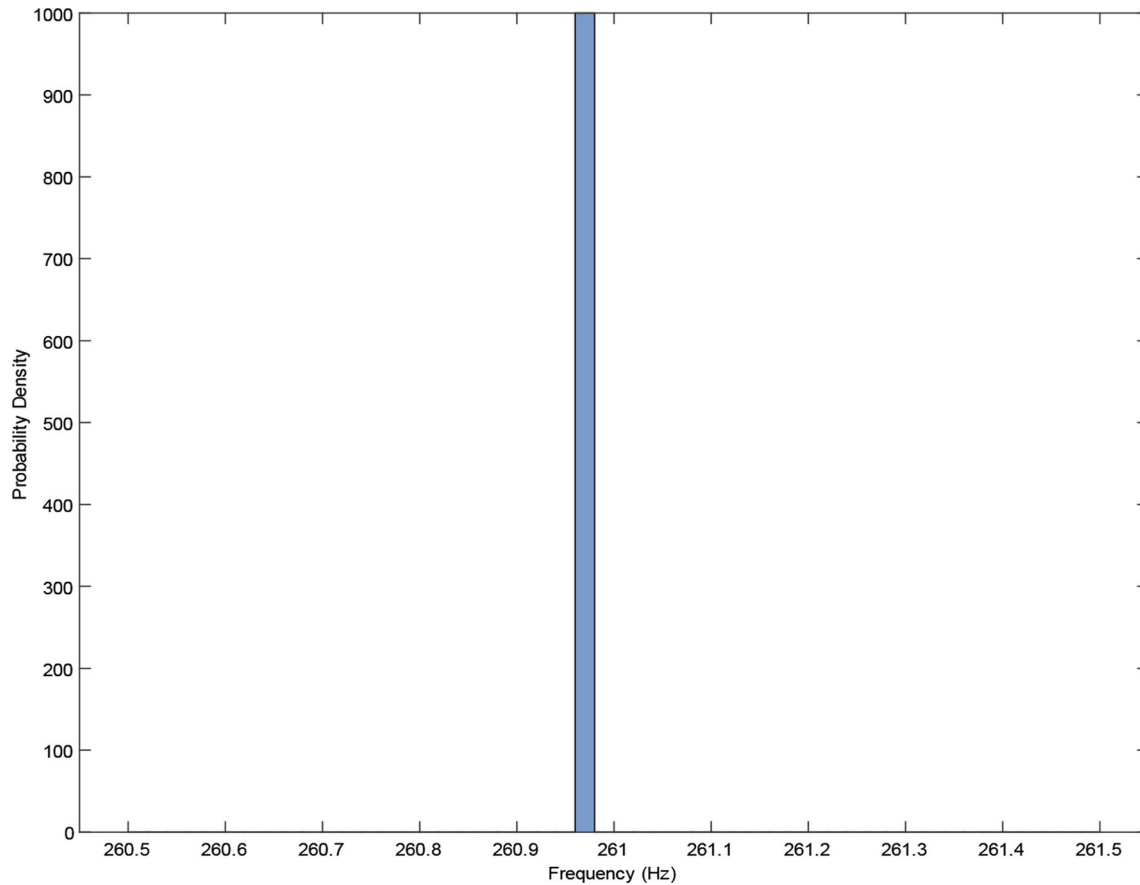
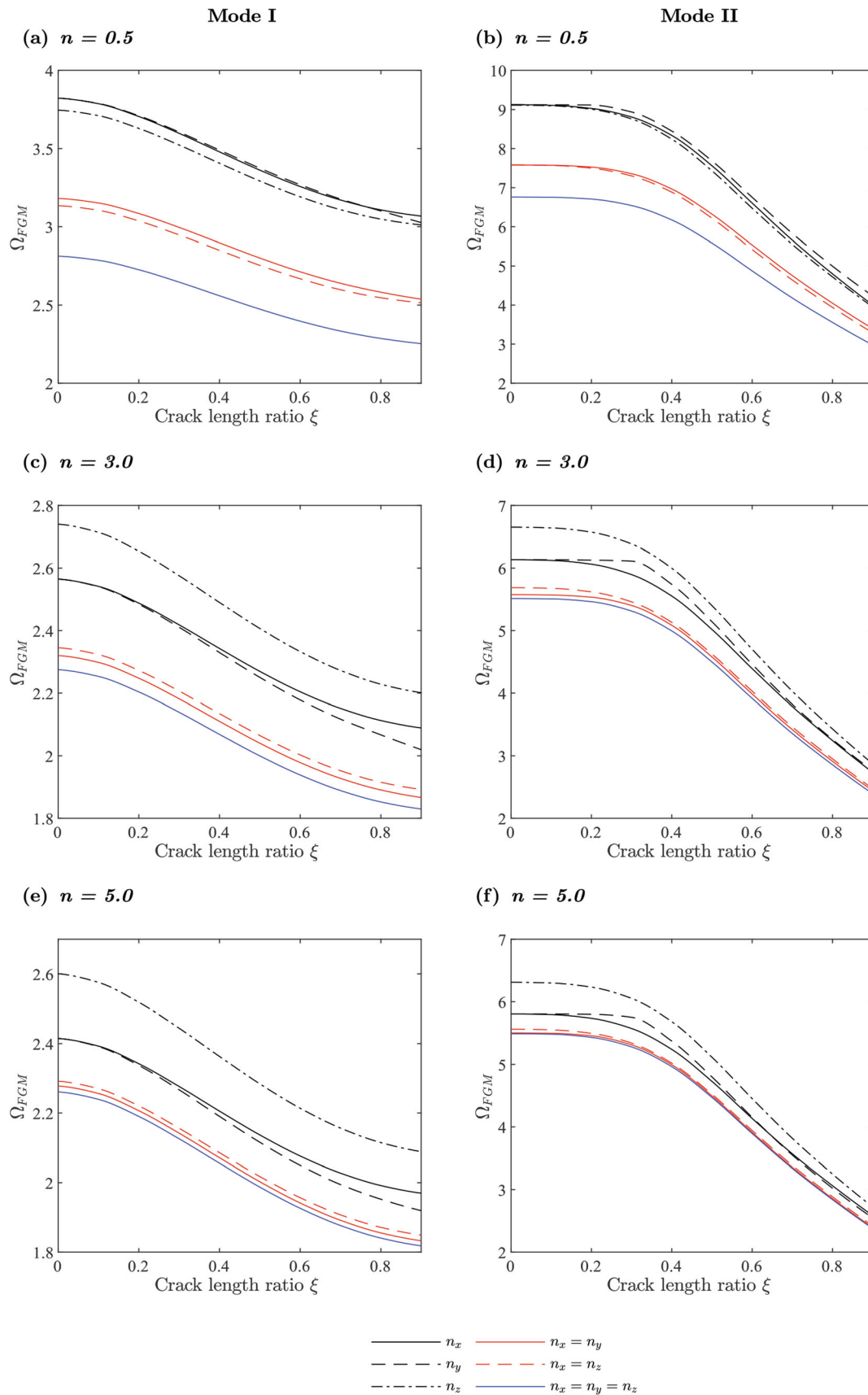


Fig. 11 Histogram of variance-based uncertainty analysis using Monte Carlo method. The input parameters are the variation of plate length, width, and thickness by approximately 1%

Samples

Square samples made of commercial carbon steel are used in the experimental work. The dimensions of the plate in the x -direction and y -direction are $a = b = 200 \pm 0.5$ mm. The thickness of the samples is $h = 2 \pm 0.01$ mm. The density (ρ) was experimentally evaluated by weighing the sample and dividing by its volume. The density of the steel plate sample is $\rho = 7600 \pm 77$ kg/m³. The elastic modulus (E) is also experimentally evaluated as $E = 201.60 \pm 4.7$

GPa. This is done by calculating the first six natural frequencies at a range of elastic moduli (185 GPa–210 GPa) using modal analysis. These frequency values were used to draw a graph resulting in a straight line corresponding to each frequency; see Fig. 5. The equations of these lines relate the natural frequency with the modulus of elasticity. By substituting an experimentally obtained natural frequency in this equation, the experimental elastic modulus can be acquired.



◀ **Fig. 12** The variation of the dimensionless frequency (Ω_{FGM}) with respect to the crack length ratio (ξ) of a simply supported FGM plate. The through crack is horizontal and at the center of the plate. The first and second columns represent the first and second natural frequencies, respectively. The frequency curves in figures (a–f) are obtained using unidirectional, two-directional, and three-directional variation of the gradient index (n). A different value of (n) is used for each row of figures

Cracked samples with different crack length ratios (c/a) were prepared using an angle grinder. A suitable cutting wheel with minimal thickness was considered to control the length and the thickness of the crack. The resulted crack tips thickness did not exceed 2 mm. Uncracked and cracked samples with crack length ratios (c/a) of 0.4, 0.55, 0.7, and 0.85 were used in this experimental work. Thirteen points were marked on the surface of each plate sample at equal distances to specify both the locations of mounting the accelerometer and impacting the plate with the hammer. Intact and cracked plate samples are shown in Fig. 6.

Test Rig

A schematic diagram, shown in Fig. 7, describes the instruments used for acquiring the natural frequency of an all-free edge plate. The plate is placed on the vehicle tire representing a 4-edge free support for the plate. A piezo-electric accelerometer (Model B&K 4517) is mounted on the plate by the means of adhesives. The weight of the accelerometer is as light as 0.65 grams, so it does not affect the mass of the plate. An impact hammer (model B&K 8202) is used to impact the plate and excite the free vibration modes. This vibration signal is then captured using the prementioned accelerometer. The data acquisition system, which is consisted of an analog input module NI-9231 mounted on a CompactRIO NI-9063, receives the signal from the accelerometer. The CompactRIO is connected to a laptop with a LABVIEW software. A code was constructed to provide a user interface to monitor the acquired analog measurement data and control the input measurement parameters. The measured signals were recorded using a sampling rate of 5.120 kS/sec during a sampling time of 10 Sec. The considered sampling rate could capture natural frequencies up to 2560 Hz, which is

more than enough for capturing the first four frequencies of the plate samples, based on the sampling theorem [60]. During each measurement process, the accelerometer was placed at minimum of two points to ensure capturing as many vibration modes as possible. This is because placing the accelerometer over an expected vibration node location would cause this vibration mode to be missed. For each accelerometer location, the plate was hit three times; then, the obtained natural frequencies were averaged. The measurement data were saved in TDMS format files. The signals obtained from the frequency measurements are analyzed using NI-DIAdem software which perform fast Fourier transform (FFT) on the signal.

Results

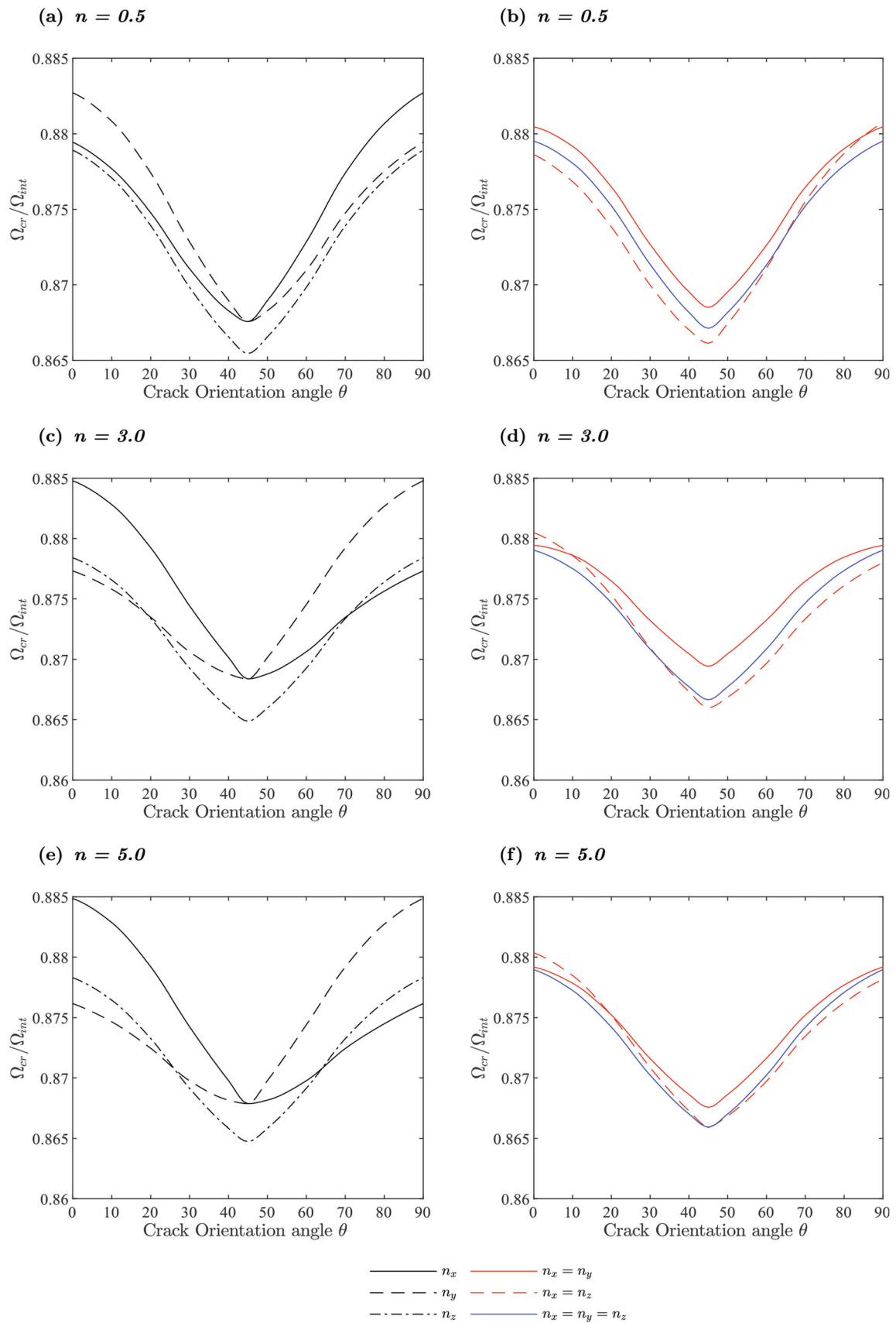
The results section consists of two subsections. The first subsection contains the validation of the FEM results of isotropic plates with experimentally obtained results. Also, the validation of the numerical formulation developed in this study with the previous literature is shown. The second subsection discusses the new results of FGM cracked plates using finite element models solved by ANSYS software.

In the results section, the obtained natural frequencies are presented as dimensionless parameters that can be calculated as follows:

$$\Omega_{FGM} = \hat{\omega} \frac{b^2}{h} \sqrt{\frac{\rho_c}{E_c}}, \tag{Eq 13}$$

$$\Omega_{Iso} = \hat{\omega} a^2 \sqrt{\frac{\rho_{Iso} h}{D_{Iso}}}, \text{ where } D_{Iso} = \frac{E_{Iso} h^3}{12(1 - \nu_{Iso}^2)}. \tag{Eq 14}$$

In the previous equations, Ω_{FGM} and Ω_{Iso} are the dimensionless frequency of the FGM and the isotropic plate, respectively. D_{Iso} is the flexural rigidity of an isotropic plate. E_{Iso} , ρ_{Iso} , and ν_{Iso} are the modulus of elasticity, density, and Poisson’s ratio of an isotropic plate. Also, the dimensionless quantities of $\xi = \frac{c}{a}$ and $\delta_c = \frac{d}{b}$ are employed in the present work, where ξ is the dimensionless crack length ratio, δ_c is the dimensionless crack position ratio, c is the crack length, and d is the vertical distance from the horizontal edge of the plate to the crack location. The dimensions d and c are illustrated in Fig. 8a, b, and c.



◀ **Fig. 13** The first natural frequency, presented as the cracked dimensionless frequency ratio $\left(\frac{\Omega_{cr}}{\Omega_{int}}\right)$, with respect to the crack orientation (θ) of a simply supported FGM plate. The through crack has a crack length ratio (ξ) of 0.5 and at an angle θ with the x-axis direction. The first and second columns represent the unidirectional and multidirectional variation of the gradient index (n), respectively. A different value of (n) is used for each row of figures

Validation of the Present Model

To verify the accuracy of the present FEM model, the validation process is conducted in two steps. First, the obtained natural frequencies from the finite elements' model are compared to the experimentally measured frequencies. This is shown in Table 1. The frequencies are presented as nondimensional frequency parameters Ω_{iso} . This is done for different crack length ratios (ξ) of [0.25, 0.4, 0.55, 0.70, 0.85]. The properties and dimensions of the isotropic plate under study are mentioned in samples. The FEM analysis in ANSYS is done using solid elements SOLID185 and shell elements SHELL181. It can be noted that the difference between the results from SOLID185 and SHELL181 is negligible as the plate is thin. There is a very good agreement between the experimental and FEM results.

In addition to the step-one validation with the experimental analysis, the model is validated with previous work in the literature in step two. The first four natural frequencies of a FGM plate are compared with the results from Talha and Singh [41] in Tables 2 and 3. The plate has an aspect ratio $\frac{a}{h}$ of 10 and is constrained with a simply supported and clamped boundary condition in Tables 2 and 3, respectively. The properties are varying in the z -direction only for values of $n_z = [0, 0.5, 1.0, 5.0, 10]$. The natural frequencies are calculated using ANSYS and employing SOLID185 and SHELL181 elements. Also, MATLAB results by applying the FSDT steps mentioned in section "Theoretical Model and Experimental Analysis" are included in the table. The number of the used solid elements is 16000, while the number of shell elements is only 1600.

Vibration of the Cracked FGM Plate

The free vibration of intact and cracked FGM (SUS304/Si3N4) plates is investigated in this section. In the first subsection, the effect of changing the material properties' direction on intact, simply supported FGM plates is studied. Then, in the following subsections, different cases of through-cracked FGM plates, shown in Fig. 8, are discussed. The plate under study is square and thick plate where $a = b = 100$ and $h = 10$. The properties of the ceramic and metal constituents are mentioned in Table 4.

Effect of Applying Unidirectional and Multidirectional Functionally Graded Material Properties on an Intact Plate

The effect of the unidirectional variation, see Fig. 2, of the gradient index (n) on the dimensionless frequency of the FGM plate (Ω_{FGM}), is shown in Fig. 9. The plate under study is an intact, thick, simply supported (SSSS) square plate. The properties of material, obtained from Eq. 2, are based on the variation of the gradient index along the x -direction (n_x), shown in Fig. 9a. On the other hand, the properties are based on variation of the gradient along the z -direction (n_z) in Fig. 9b. The effect of changing the elastic modulus (E_{FGM}) and the density (ρ_{FGM}) separately on the dimensionless frequency (Ω_{FGM}) is also demonstrated in the figure for both the x - and z -directions. The frequency is calculated based on changing the elastic modulus while keeping the density constant and equal to the metal density (ρ_m) once, then based on changing the density while fixing the elastic modulus to the metal's modulus (E_m).

It is observed from Fig. 9 that the dimensionless frequency (Ω_{FGM}) generally decreases as the gradient indices (n_x and n_z) increase. This is due to the decrease of the ceramic's volume as n increases which results in reduction of the plate's stiffness. Furthermore, the decrease in frequency is sharp for values of (n_x and n_z) < 3, while it is insignificant for higher values of (n_x and n_z). Also, the density (ρ) contribution to the dimensionless frequency at low gradient indices is higher than that of the elastic modulus (E). However, the difference between the frequencies in the two cases decreases as the gradient index

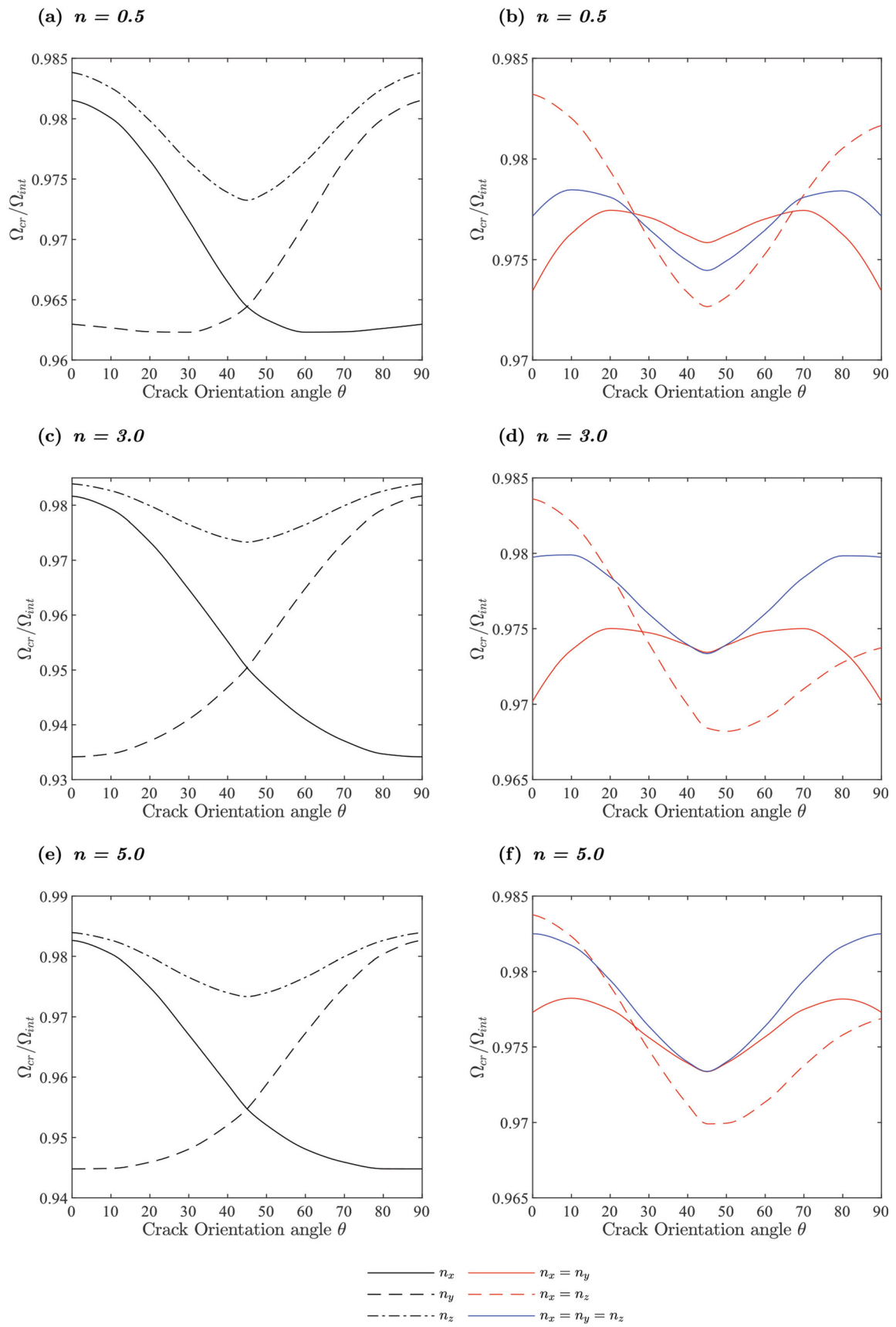


Fig. 14 The third natural frequency, presented as the cracked dimensionless frequency ratio $\left(\frac{\Omega_{cr}}{\Omega_{int}}\right)$, with respect to the crack orientation (θ) of a simply supported FGM plate. The through crack has a crack length ratio (ζ) of 0.5 and at an angle θ with the x -axis direction. The first and second columns represent the unidirectional and multidirectional variation of the gradient index (n), respectively. A different value of (n) is used for each row of figures

increases until the contribution effect is reversed eventually.

A comparison between the frequency ratios $\left(\frac{\Omega_{FGM}}{\Omega_{iso}}\right)$ resulting from the unidirectional, two-directional, and three-directional variation of the gradient index (n) is illustrated in Fig. 10. The unidirectional variation of the gradient index is along the x -direction (n_x) and the z -direction (n_z) separately. The two-directional variation of the gradient index is along the plate's in-plane directions (n_x, n_y) and the $x - z$ plane of the plate (n_x, n_z). Finally, the three-directional variation of the gradient index is along all the three directions (n_x, n_y, n_z). The first- and second-plate natural frequencies for each variation direction of the gradient index are shown in Fig. 10a and b, respectively. One can conclude from the figure that for all values of (n) the unidirectional variation of material properties resulted in the highest natural frequency. In contrast, the lowest natural frequency was caused by the three-directional variation.

To deal with uncertainties in the input parameters, a variance-based uncertainty analysis using the Monte Carlo method was performed in the numerical simulations, see Fig. 11. The input parameters considered were the plate's length, width, and thickness. These parameters can exhibit variations due to manufacturing tolerances in the range of 1%. There are a large number of random samples for the input parameters by sampling from their normal probability distributions. For the set of input samples, numerical simulations were conducted to obtain the corresponding plate natural frequencies as outputs. It is found that the plate's natural frequency remained approximately unchanged. The variance-based uncertainty analysis allows gaining insights into the sensitivity of the output to variations in each input parameter.

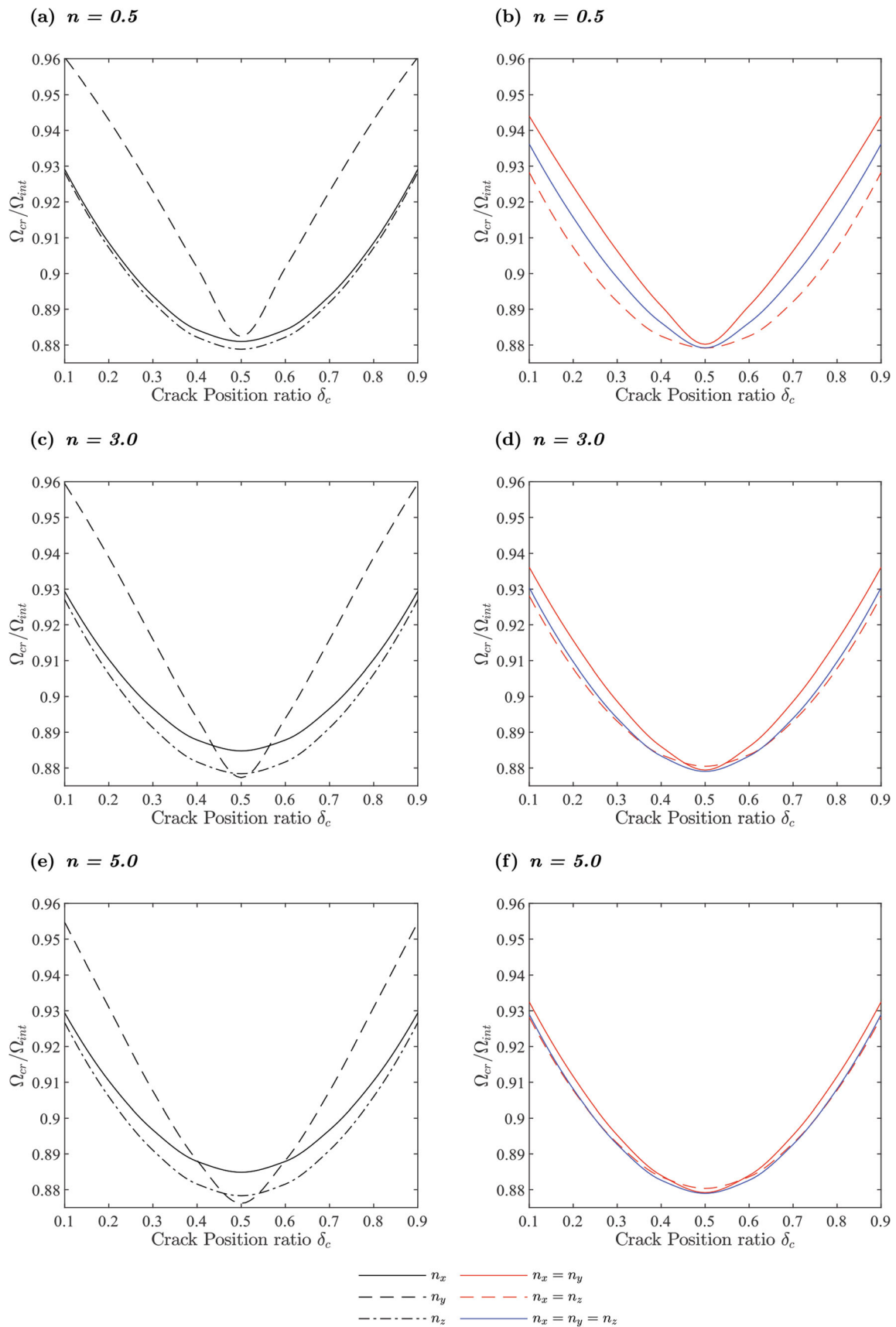
Effect of Crack Length on Unidirectional and Multidirectional Functionally Graded Material-Cracked Plate

The influence of the crack length ratio (ζ) on the dimensionless frequency (Ω_{FGM}) using different values of gradient index (n) is shown in Fig. 12. The used values of

the crack length ratio (ζ) are from 0.10 to 0.90 with a step of 0.10. The first and second columns represent the first and second natural frequencies, respectively. The frequency curves in each row are based on different values of the gradient index, namely $n = 0.5, 3.0, 5.0$ in an ascending arrangement. For each value of n , frequency is calculated based on unidirectional, two-directional, and three-directional variation of the gradient index. It can be seen in the figure that the increase in the crack length results in reducing the stiffness of the plate, thus decreasing the natural frequency in all cases as expected. However, the rate of decreasing is the dimensionless natural frequency was higher in the second mode compared with that of the first mode.

Effect of Crack Orientation on Unidirectional and Multidirectional Functionally Graded Material-Cracked Plate

The influence of changing the orientation of the crack on the first and third natural frequencies of a (SSSS) plate is illustrated in Figs. 13 and 14, respectively. The figures show the natural frequency, presented as the cracked dimensionless frequency ratio $\left(\frac{\Omega_{cr}}{\Omega_{int}}\right)$, with respect to the crack orientation (θ) of a simply supported FGM plate. Both the dimensionless frequency of the cracked FGM (Ω_{cr}) and of the intact FGM plate (Ω_{int}) can be calculated from Eq. 13. The through crack has a crack length ratio (ζ) of 0.5 and at an angle θ with the x -axis direction. The first and second columns represent the unidirectional and multidirectional variation of the gradient index n , respectively. A different value of n is used for each row of figures. The natural frequencies are presented as cracked dimensionless frequency ratio $\left(\frac{\Omega_{cr}}{\Omega_{int}}\right)$ on the y -axis. The through crack is inclined, and its center is aligned with the plate's center. Crack orientation angles (θ) of (0, 10, 20, 30, 40, 45, 50, 60, 70, 80, 90) are used where the angle is measured from the x -axis, see Fig. 8b. The first column of figures is obtained using unidirectional variation of the gradient index, while the second column is obtained using two-directional and three-directional variation of the gradient index. The gradient index for each row of figures is constant and increases while moving downward. Gradient index values of $n = 0.5, 3.0$ and 5.0 are used in this case study. It can be noted that the lowest frequency occurs at $\theta = 45^\circ$ in the case of the first natural frequency. On the other hand, the lowest frequencies in the case of the third natural frequency differ depending on the direction of the gradient index variation and its value. It can also be realized that the relatively lowest first frequency was in case of n_z only as shown in Fig 13. However, the situation is



◀ **Fig. 15** The first natural frequency of a simply supported FGM plate with respect to different crack position ratios (δ_c). The frequency is represented as the dimensionless frequency ratio ($\frac{\Omega_{cr}}{\Omega_{in}}$). The frequency curves in each figure (a–c) are obtained using unidirectional and two-directional variation of gradient index with values corresponding to 0.5, 3.0, and 5.0, respectively

completely reversed in the third mode as shown in Fig. 14. Also, the case $n_x = n_y$ shows the highest first mode in frequency compared with the other multidirectional variation. Again, the situation differs in the third mode. This may be explained by the fact that the different frequencies have different mode shapes which interacts with the distribution of the FGM and the crack orientation as well.

Effect of Crack Position on Unidirectional and Multidirectional Functionally Graded Material-Cracked Plate

The effect of changing the dimensionless crack position ratio (δ_c) on the cracked dimensionless frequency ratio ($\frac{\Omega_{cr}}{\Omega_{in}}$) of a simply supported and a cantilever square plate is discussed in Figs. 15 and 16, respectively. The crack length ratio (ζ) of the crack in the plate model equals 0.5. The used values of the crack length ratio (δ_c) are from 0.10 to 0.90 with a step of 0.10. It is noted from Fig. 15 that the first natural frequency is at its minimum value when the crack is at the center of the simply supported plate.

The value of the frequency increases as the crack moves toward the edges of the plate. In the case of a cantilever plate Fig. 16, the lowest frequency is obtained when the crack is closest to the fixed edge. Furthermore, the effect of

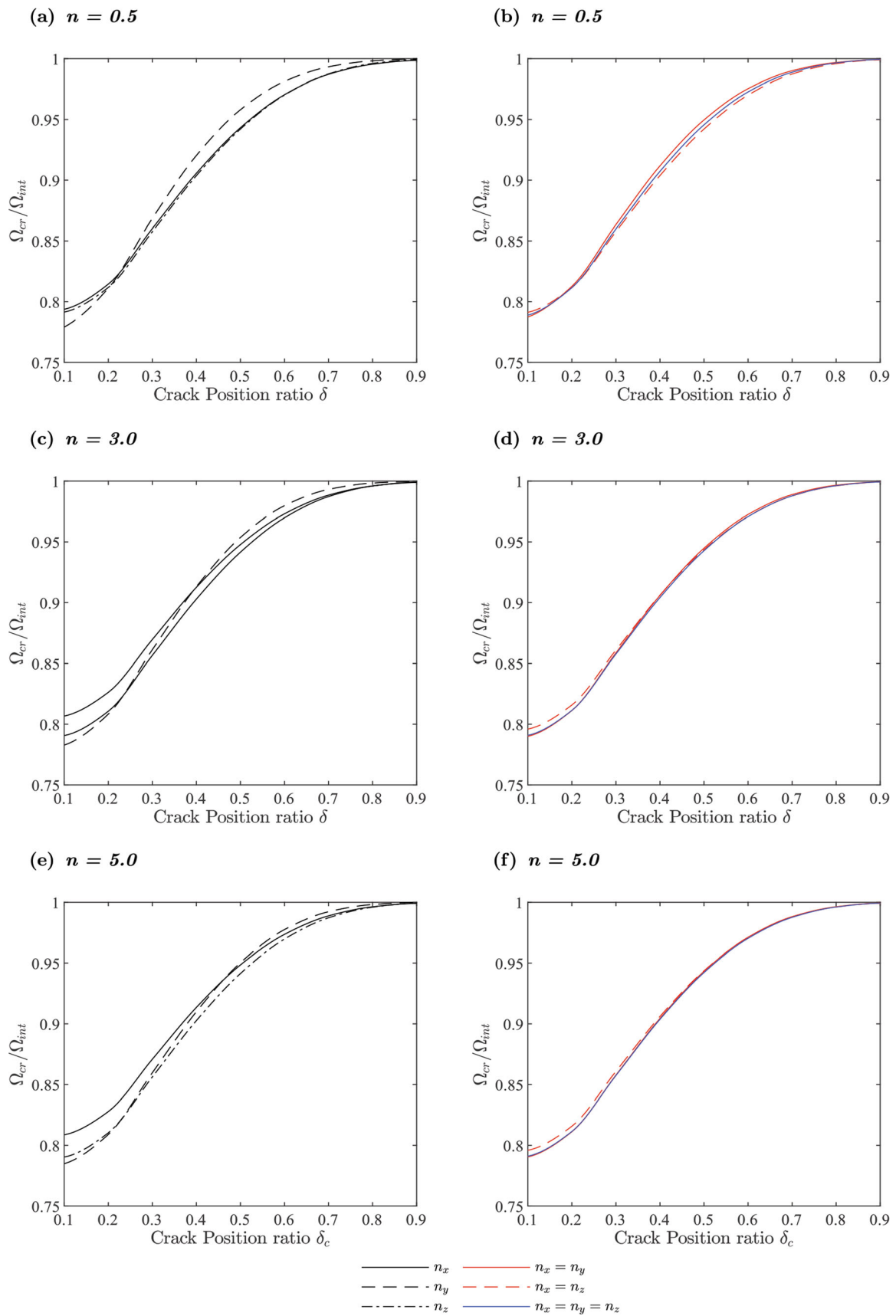
two- and three-directional variation of the gradient index is insignificant, and the frequency obtained is almost identical.

Finally, it is crucial to acknowledge the limitations of the present analysis after presenting the model results. Firstly, the experimental results are limited to isotropic materials. Secondly, the numerical code utilized in this study is specifically designed for intact materials and does not incorporate the effects of cracks. Lastly, the results obtained from the ANSYS code encompass all the physics considered in the present analysis, indicating that the chosen software adequately captures the relevant phenomena for the studied problem.

Conclusion

In this paper, the free vibration of functionally graded intact and cracked plates is investigated. The analysis is based on numerical and experimental analysis. The experimental work is used to identify the plate material properties and to validate the results of the numerical model in the case of isotropic cracked plate. The numerical model is based on finite element analysis using both MATLAB code for uncracked samples and ANSYS software package for the case of cracked FGM. A code is prepared to model two- and three-directional material distribution in plates in ANSYS mechanical APDL. This enables a novel study of the combined effects resulting from variations in FGM material properties, crack length, crack orientation, and crack location.

The experimental results verified the finite element model in the case of isotropic materials. The variance-based uncertainty analysis using the Monte Carlo method



◀**Fig. 16** The first natural frequency of a cantilever FGM plate with respect to different crack position ratios (δ_c). The frequency is represented as the dimensionless frequency ratio ($\frac{\omega}{\omega_{int}}$). The frequency curves in each figure (a–c) are obtained using unidirectional and two-directional variation of gradient index with values corresponding to 0.5, 3.0, 5.0, respectively

results indicates the possible manufacturing imperfection has minor effect on the plate dynamics. Also, the results show the effect of changing the FGM properties in the three directions on the intact plates. It was shown that the use of FGM in the three directions reveals the lowest natural frequency in the first and second mode as shown in Fig. 10. The results show also that the FGM gradient affects the plate natural frequencies greatly when $n < 3$. Higher than that the FGM gradient approaches to have no effect on both cracked and intact plates. The results also show the effect of crack location on the plated depends on the boundary condition of plates. Finally, the results of the present manuscript can guide to the design based on FGM plates, especially when cracks exist.

Open Access This article is licensed under a Creative Commons Attribution 4.0 International License, which permits use, sharing, adaptation, distribution and reproduction in any medium or format, as long as you give appropriate credit to the original author(s) and the source, provide a link to the Creative Commons licence, and indicate if changes were made. The images or other third party material in this article are included in the article’s Creative Commons licence, unless indicated otherwise in a credit line to the material. If material is not included in the article’s Creative Commons licence and your intended use is not permitted by statutory regulation or exceeds the permitted use, you will need to obtain permission directly from the copyright holder. To view a copy of this licence, visit <http://creativecommons.org/licenses/by/4.0/>.

Data Availability The raw/processed data required to reproduce these findings cannot be shared at this time as the data also form part of an ongoing study.

Appendix

See Fig. 17.

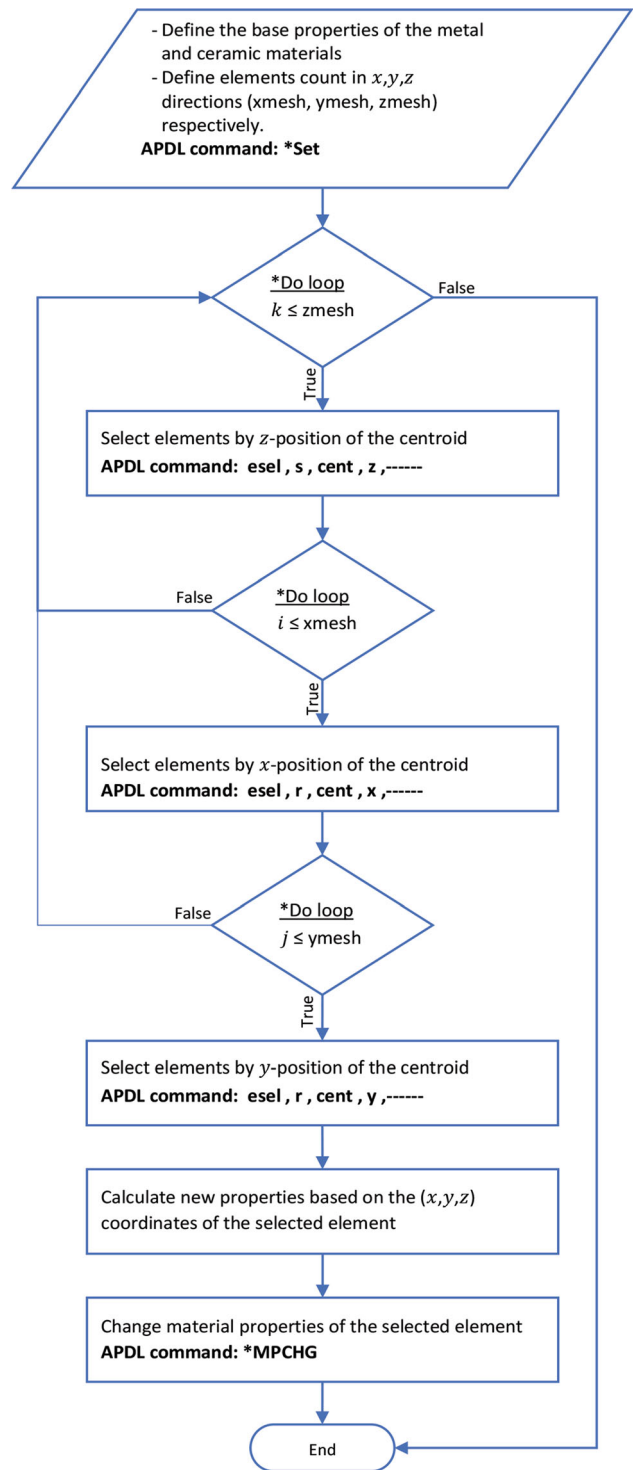


Fig. 17 A flow chart explaining the APDL coding procedure of selecting the elements and assigning the corresponding material properties

References

1. M. Koizumi, The concept of FGM. *Ceram. Trans.* **34**, 3–10 (1993)
2. A.W. Leissa, *Vibration of plates*, Scientific and Technical Information Division, National Aeronautics and (1969)
3. R. Szilard, Theories and applications of plate analysis: classical, numerical and engineering methods. *J Appl. Mech. Rev.* **57**, B32–B33 (2004)
4. C.M. Wang, J.N. Reddy, K.H. Lee, *Shear deformable beams and plates: Relationships with classical solutions*, Elsevier (2000)
5. J.N. Reddy, *Theory and Analysis of Elastic Plates and Shells*, CRC Press, (2006)
6. R.D. Mindlin, Influence of rotatory inertia and shear on flexural motions of isotropic, elastic plates. *J. Appl. Mech.* **18**, 31–38 (1951)
7. M. Levinson, An accurate, simple theory of the statics and dynamics of elastic plates. *Mech. Res. Commun.* **7**, 343–350 (1980)
8. K.H. Lo, R.M. Christensen, E.M. Wu, A high-order theory of plate deformation—part 1: homogeneous plates. *J. Appl. Mech.* **44**, 663–668 (1977)
9. N.F. Hanna, A.W. Leissa, A higher order shear deformation theory for the vibration of thick plates. *J. Sound Vib.* **170**, 545–555 (1994)
10. Taima MS, El-Sayed TA, Shehab MB, Farghaly SH, Hand RJ. Vibration analysis of cracked beam based on Reddy beam theory by finite element method. *Journal of Vibration and Control.* (2022) 10775463221122122
11. T. El-Sayed, R.J. Hand, Modelling the strengthening of glass using epoxy based coatings. *J. Eur. Ceram. Soc.* **31**, 2783–2791 (2011)
12. B. Stahl, L.M. Keer, Vibration and stability of cracked rectangular plates. *Int. J. Solids Struct.* **8**, 69–91 (1972)
13. S.E. Khadem, M. Rezaee, An analytical approach for obtaining the location and depth of an all-over part-through crack on externally in-plane loaded rectangular plate using vibration analysis. *J. Sound Vib.* **230**, 291–308 (2000)
14. D.Y. Liu, C.Y. Wang, W.Q. Chen, Free vibration of FGM plates with in-plane material inhomogeneity. *Compos. Struct.* **92**, 1047–1051 (2010)
15. R. Meksi, S. Benyoucef, A. Mahmoudi, A. Tounsi, E.A. Adda Bedia, S.R. Mahmoud, An analytical solution for bending, buckling and vibration responses of FGM sandwich plates. *J. Sandw. Struct. Mater.* **2**, 727–757 (2019)
16. J.R. Rice, N. Levy, The part-through surface crack in an elastic plate. (1972)
17. F. Delale, F. Erdogan, Line-spring model for surface cracks in a Reissner plate. *Int. J. Eng. Sci.* **19**, 1331–1340 (1981)
18. Z. Zhao-Jing, D. Shu-Ho, Stress intensity factors for an inclined surface crack under biaxial stress state. *J. Eng. Fract. Mech.* **47**, 281–289 (1994)
19. P. Joseph, F. Erdogan, Surface crack in a plate under antisymmetric loading conditions. *Int. J. Solids Struct.* **27**, 725–750 (1991)
20. A. Israr, M.P. Cartmell, E. Manoach, I. Trendafilova, W. Ostachowicz, M. Krawczuk, A. Żak, Analytical modeling and vibration analysis of partially cracked rectangular plates with different boundary conditions and loading, *Journal of Applied Mechanics*, 76 (2009)
21. R. Ismail, M. Cartmell, An investigation into the vibration analysis of a plate with a surface crack of variable angular orientation. *J. Sound Vib.* **331**, 2929–2948 (2012)
22. T. Bose, A. Mohanty, Vibration analysis of a rectangular thin isotropic plate with a part-through surface crack of arbitrary orientation and position. *J. Sound Vib.* **332**, 7123–7141 (2013)
23. P.V. Joshi, N.K. Jain, G.D. Ramtekkar, Analytical modelling for vibration analysis of partially cracked orthotropic rectangular plates. *Eur. J. Mech. A. Solids.* **50**, 100–111 (2015)
24. P.V. Joshi, N.K. Jain, G.D. Ramtekkar, Analytical modeling for vibration analysis of thin rectangular orthotropic/functionally graded plates with an internal crack. *J. Sound Vib.* **344**, 377–398 (2015)
25. A. Gupta, N.K. Jain, R. Salhotra, Effect of crack orientation on vibration characteristics of partially cracked FGM plate: An analytical approach. *Mater. Today Proc.* **4**, 10179–10183 (2017)
26. A. Gupta, N.K. Jain, R. Salhotra, P.V. Joshi, S. Soni, Effect of crack location on vibration analysis of cracked FGM plate under thermal environment. *Mater. Today Proc.* **5**, 28043–28050 (2018)
27. S. Soni, N.K. Jain, P.V. Joshi, A. Gupta, Effect of thermal environment on vibration response of partially cracked functionally graded plate coupled with fluid. *Mater. Today Proc.* **5**, 27810–27819 (2018)
28. G. Aksu, R. Ali, Free vibration analysis of stiffened plates using finite difference method. *J. Sound Vib.* **48**, 15–25 (1976)
29. G. Aksu, R. Ali, Determination of dynamic characteristics of rectangular plates with cutouts using a finite difference formulation. *J. Sound Vib.* **44**, 147–158 (1976)
30. K.S. Numayr, R.H. Haddad, M.A. Haddad, Free vibration of composite plates using the finite difference method. *Thin-Walled Struct.* **42**, 399–414 (2004)
31. C.S. Huang, A. Leissa, Vibration analysis of rectangular plates with side cracks via the Ritz method. *J. Sound Vib.* **323**, 974–988 (2009)
32. C.S. Huang, A. Leissa, R. Li, Accurate vibration analysis of thick, cracked rectangular plates. *J. Sound Vib.* **330**, 2079–2093 (2011)
33. C.S. Huang, A.W. Leissa, C.W. Chan, Vibrations of rectangular plates with internal cracks or slits. *Int. J. Mech. Sci.* **53**, 436–445 (2011)
34. C.S. Huang, O.G. McGee, M.J. Chang, Vibrations of cracked rectangular FGM thick plates. *Compos. Struct.* **93**, 1747–1764 (2011)
35. B. Uymaz, M. Aydogdu, S. Filiz, Vibration analyses of FGM plates with in-plane material inhomogeneity by Ritz method. *Compos. Struct.* **94**, 1398–1405 (2012)
36. Q. Guan-Liang, G. Song-Nian, J. Jie-Sheng, A finite element model of cracked plates and application to vibration problems. *Comput. Struct.* **39**, 483–487 (1991)
37. M. Krawczuk, Gdansk, Natural vibrations of rectangular plates with a through crack. *Arch. Appl. Mech.* **63**, 491–504 (1993)
38. M. Krawczuk, W.M. Ostachowicz, A finite plate element for dynamic analysis of a cracked plate. *Comput. Methods Appl. Mech. Eng.* **115**, 67–78 (1994)
39. M.S. Azam, V. Ranjan, B. Kumar, Finite element modelling and analysis of free vibration of a square plate with side crack. *Differ. Equ. Dyn. Syst.* **29**, 299–311 (2021)
40. J. Reddy, Analysis of functionally graded plates. *Int. J. Numer. Methods Eng.* **47**, 663–684 (2000)
41. M. Talha, B.N. Singh, Static response and free vibration analysis of FGM plates using higher order shear deformation theory. *Appl. Math. Model.* **34**, 3991–4011 (2010)
42. P.P. Minh, D.T. Manh, N.D. Duc, Free vibration of cracked FGM plates with variable thickness resting on elastic foundations. *Thin-Walled Struct.* **161**, 107425 (2021)
43. P.P. Minh, N.D. Duc, The effect of cracks and thermal environment on free vibration of FGM plates. *Thin-Walled Struct.* **159**, 107291 (2021)
44. G. Shi, A new simple third-order shear deformation theory of plates. *Int. J. Solids Struct.* **44**, 4399–4417 (2007)

45. A. Yazid, N. Abdelkader, H. Abdelmadjid, A state-of-the-art review of the X-FEM for computational fracture mechanics. *Appl. Math. Model.* **33**, 4269–4282 (2009)
46. T. Belytschko, T. Black, Elastic crack growth in finite elements with minimal remeshing. *Int. J. Numer. Meth. Eng.* **45**, 601–620 (1999)
47. J.M. Melenk, I. Babuška, The partition of unity finite element method: basic theory and applications. *Comput. Methods Appl. Mech. Eng.* **139**, 289–314 (1996)
48. N. Moës, J. Dolbow, T. Belytschko, A finite element method for crack growth without remeshing. *Int. J. Numer. Methods Eng.* **46**, 131–150 (1999)
49. M. Bachene, R. Tiberkak, S. Rechak, Vibration analysis of cracked plates using the extended finite element method. *Arch. Appl. Mech.* **79**, 249–262 (2009)
50. M. Bachene, R. Tiberkak, S. Rechak, G. Maurice, B.K. Hachi, *Enriched Finite Element for Modal Analysis of Cracked Plates* (Springer, Damage and Fracture Mechanics, 2009), p.463–471
51. S. Natarajan, P.M. Baiz, S. Bordas, T. Rabczuk, P. Kerfriden, Natural frequencies of cracked functionally graded material plates by the extended finite element method. *Compos. Struct.* **93**, 3082–3092 (2011)
52. S. Hosseini-Hashemi, H.R. Gh, DT HR. Exact free vibration study of rectangular Mindlin plates with all-over part-through open cracks. *Comput. Struct.* **88**(17), 101532 (2010)
53. P.K. Nkounhawa, D. Ndapeu, B. Kenmeugne, T. Beda, Analysis of the behavior of a square plate in free vibration by FEM in ansys, world. *J. Mech.* **10**, 11–25 (2020)
54. P. Pingulkar, B. Suresha, Free vibration analysis of laminated composite plates using finite element method. *Polym. Polym. Compos.* **24**, 529–538 (2016)
55. M.A. Al-Shammari, Experimental and FEA of the crack effects in a vibrated sandwich plate. *J. Eng. Appl. Sci.* **13**, 7395–7400 (2018)
56. S.J.S. Tabatabaei, A.M. Fattahi, A finite element method for modal analysis of FGM plates. *Mech. Based Des. Struct. Mach.* **50**, 1111–1122 (2022)
57. H. Guo, X. Zhuang, T. Rabczuk, A deep collocation method for the bending analysis of kirchhoff plate, *Comput. Mater. Contin.* **59** (2019)
58. X. Zhuang, H. Guo, N. Alajlan, H. Zhu, T. Rabczuk, Deep autoencoder based energy method for the bending, vibration, and buckling analysis of Kirchhoff plates with transfer learning. *Eur. J. Mech. A. Solids.* **87**, 104225 (2021)
59. S. Goswami, C. Anitescu, S. Chakraborty, T. Rabczuk, Transfer learning enhanced physics informed neural network for phase-field modeling of fracture. *Theoret. Appl. Fract. Mech.* **106**, 102447 (2020)
60. A. Brandt, *Noise and Vibration Analysis: Signal Analysis and Experimental Procedures*, John Wiley & Sons (2011)

Publisher's Note Springer Nature remains neutral with regard to jurisdictional claims in published maps and institutional affiliations.